Mantle source heterogeneity in a Neoproterozoic back-arc basin: Geochemical and thermodynamic modeling of the volcanic section of Wadi Ghadir ophiolite, Egypt

Basem Zoheir [a,b,*], Aliaa Diab [a], Petros Koutsovitis [c], Tamer Abu Alam [d], Mark Feigenson [e], Mohammed El-Bialy [f], Amr Abdelnasser [a]

[a] Department of Geology, Faculty of Science, Benha University, 13518 Benha, Egypt
[b] Institute of Geosciences, University of Kiel, Ludewig-Meyn Str. 10, 24118 Kiel, Germany
[c] Department of Geology, University of Patras, 26504 Rio Patra, Greece
[d] The Faculty of Biosciences, Fisheries and Economics, University of Tromsø - the Arctic University of Norway, 9037 Tromsø, Norway
[e] Department of Earth and Planetary Sciences, Wright-Rieman Labs, Rutgers University, Piscataway, NJ, USA
[f] Geology Department, Faculty of Science, Port Said University, 42522 Port Said, Egypt

ARTICLE INFO

Keywords:
Neoproterozoic ophiolite
Arabian-Nubian Shield
Primary melt composition
Thermodynamic modeling
Mantle source heterogeneity
Marginal oceanic basin

ABSTRACT

Wadi Ghadir ophiolite in the Egyptian Eastern Desert, which forms the northern part of the Nubian Shield, is considered as one of the best-preserved segments of the Neoproterozoic oceanic lithosphere on Earth. Primary melt calculations and thermodynamic modeling of new geochemical data for the Wadi Ghadir pillow lavas and dike complexes, integrated with comprehensive petrographic investigations, are here employed to unravel the geodynamic evolution of this ophiolitic section.

Whole-rock geochemical and clinopyroxene data indicate that the pillow lavas and sheeted dike complexes preserve geochemical signatures of N-MORB, E-MORB and OIB-like basalts. Less abundant, discrete dikes have a distinctly LILE-enriched island arc tholeiite (IAT) composition. The pillow lavas and sheeted dike complexes replicate mixed liquid lines of descent, whereas the discrete dikes exhibit a calc-alkaline differentiation trend. The pillow lavas were produced by limited (5–7%) mantle partial melting as a result of isothermal decompression over a wide pressure range (5 – 19 kbar) and restricted mantle potential temperatures (Tp ≈ 1260–1300 °C), suggesting ponding of rising melts from depths of ~60 to 15 km in dry mantle. Primary melts of the sheeted dike complexes were produced by 9–11% partial melting at P ≈ 9.7 ± 2.5 kbar, Tp ≈ 1290 °C, and P ≈ 14.7 ± 1.4 kbar, Tp ≈ 1325 °C, suggesting a role of varying hydrostatic pressure. The magma source for the discrete dikes occurred at 10.7 ± 0.6 kbar and Tp of 1230–1300 °C by 11–13% partial melting of a metasomatized mantle region.

The calculated Tp ranges for the different melts are consistently lower than temperatures of sub-ridge ambient mantle. Together with the variable concentrations of K_2O and other incompatible elements, the estimated low temperatures of melt generation emphasize mixed sources and wet peridotite melting. The modeled primary melts designate crustal growth during back-arc basin opening and closure. During the basin opening, decompression melting of mildly enriched mantle produced high-Ti tholeiitic (pillow lavas) and transitional (sheeted dike complexes) melts, whereas subduction initiation during basin closure promoted melt-peridotite interaction. Lowering of the solidus by subduction-related components triggered melting of a spinel lherzolitic mantle and produced low-Ti calc-alkaline melts that sourced the discrete dikes. The mixed MORB and SSZ geochemical characteristics of the studied volcanic rocks, coupled with the various modeled melts and lack of significant thermal anomalies in the mantle conditions, are here interpreted as manifestations of mantle source heterogeneity in a marginal oceanic basin during the accretionary stages of the Arabian-Nubian Shield.

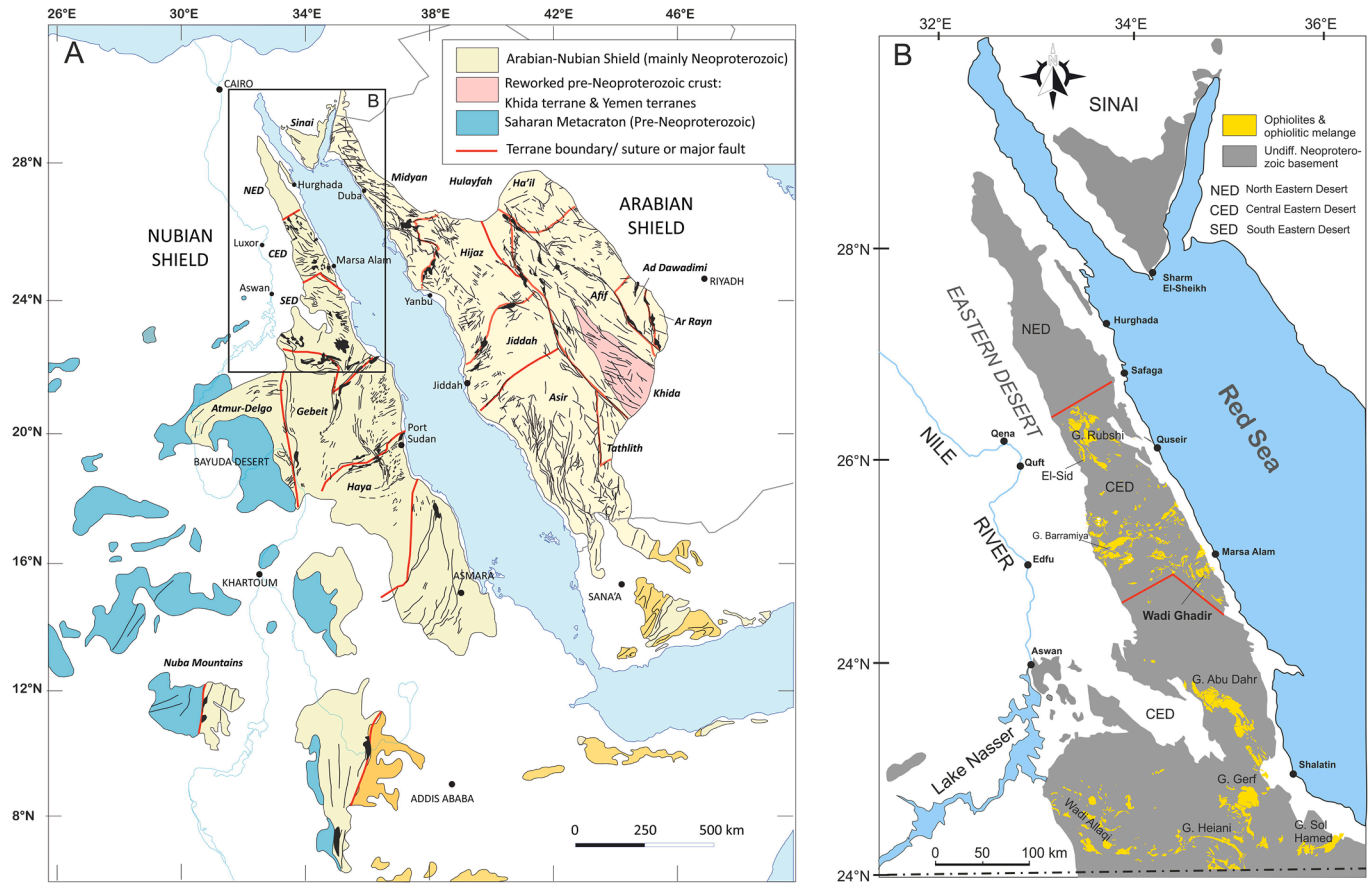

Fig. 1. (A) Major structures and ophiolite occurrences across the ANS. Notice the mutual spatial association with terrane boundaries, i.e., sutures or major wrench structures (modified from Johnson and Woldehaimanot, 2003; Shackleton, 1994), (B) Distribution of ophiolite nappes and mélange in the Eastern Desert of Egypt (based on published geological maps of Conoco Coral, 1987; EGSMA, 1997).

1. Introduction

Geochemical diversity of ophiolitic rocks is commonly attributed to the extent and type of magmatic processes operating in the ascending or residing melts at the different crustal levels. In a supra-subduction zone setting, melts generated by partial melting of different mantle sources also contribute to the heterogeneity of ophiolitic rocks (e.g., Dilek et al., 2008; Metcalf and Shervais, 2015; Koutsovitis and Magganas, 2016; Rogkala et al., 2019; Golich and Vysotskiy, 2020). The magmatic and geochemical evolution of supra-subduction zone (SSZ) and volcanic arc (VA) ophiolites are largely controlled by the mode and nature of mantle melting. Other factors include the distance from the subducting slab and mobile components released by dehydration and decarbonation of the descending sediment veneers and/or metasomatized mafic rocks (Tsikouras et al., 2009), as well as the vertical gradation within the melting mantle column (e.g., Dilek et al., 2008). An ophiolite volcanic section commonly preserves magmatic progression from less to more HFSE-depleted and LILE-enriched compositions. This variation is most likely linked with subduction initiation as a switch from extensional to compressional environment (Whattman and Stern, 2011). Progression from MORB to IAT affinities is explained by the subduction-related inputs, whereas ophiolites recording evolution from IAT to MORB compositions are related to opening of back-arc basins (e.g., Bortolotti, 2002). Herzberg et al. (2007) suggested that small variations in mantle source temperatures can induce large variations in the major element composition of primary melts for ophiolitic volcanic rocks, where MgO evolves with increasing potential temperatures of the ambient mantle.

Considering their large outcrops and conspicuous abundance in many orogenic belts, ophiolites provide an excellent opportunity to study melting processes in the MOR and subduction settings throughout the geological time. The Arabian-Nubian Shield (ANS) is a large and well-exposed, long-lived accretionary belt recording cycles of oceanic basin formation, subduction, crustal thickening and orogen collapse in the Neoproterozoic era (e.g., Kusky et al., 2003; Kröner and Stern, 2004; Johnson et al., 2011). The ANS was developed when terranes of arc and back-arc crust accreted within and around the margins of a large oceanic tract known as the Mozambique Ocean (e.g., Fritz et al., 2013 and references therein). The latter was created when the breakup of Rodinia took place at ~900–800 Ma (Stern et al., 2004). Subduction zones, commonly marked by ophiolitic sections (mostly dissmembered) and ophiolitic mélange rocks were obducted onto the continental crust during the amalgamation of the ANS (e.g., Stern, 2004; Johnson et al., 2011). Ophiolitic rocks (~890–700 Ma) form a major component in the ANS, underlying extensive areas and commonly occur in association with island arc volanic/volcaniclastic sequences (e.g., Abdelsalam et al., 2003; Stern et al., 2004; Ali et al., 2010).

Despite the large number of publications, the genesis and evolution of the ANS ophiolites and their tectonic setting remain enigmatic. Metamorphic soles at the basal contact of scattered ophiolites with tectonically lower gneissic rocks in the Eastern Desert of Egypt (Abd El-Naby et al., 2008) indicate that emplacement of the ANS ophiolites occurred shortly after its formation. Cold emplacement of ophiolitic blocks in the shield is also deduced from the widespread low or medium grade of metamorphism of their footwall island arc rocks (e.g., Stern, 2004; Zoheir and Klemm, 2007). Numerous studies interpret most of the ANS ophiolite sections as SSZ ophiolites (Abdel-Karim et al., 2001; Stern et al., 2004; Abd El-Rahman et al., 2009a,b, 2012 and references therein), while Zimmer et al. (1995) described a mid-ocean ridge (MOR)

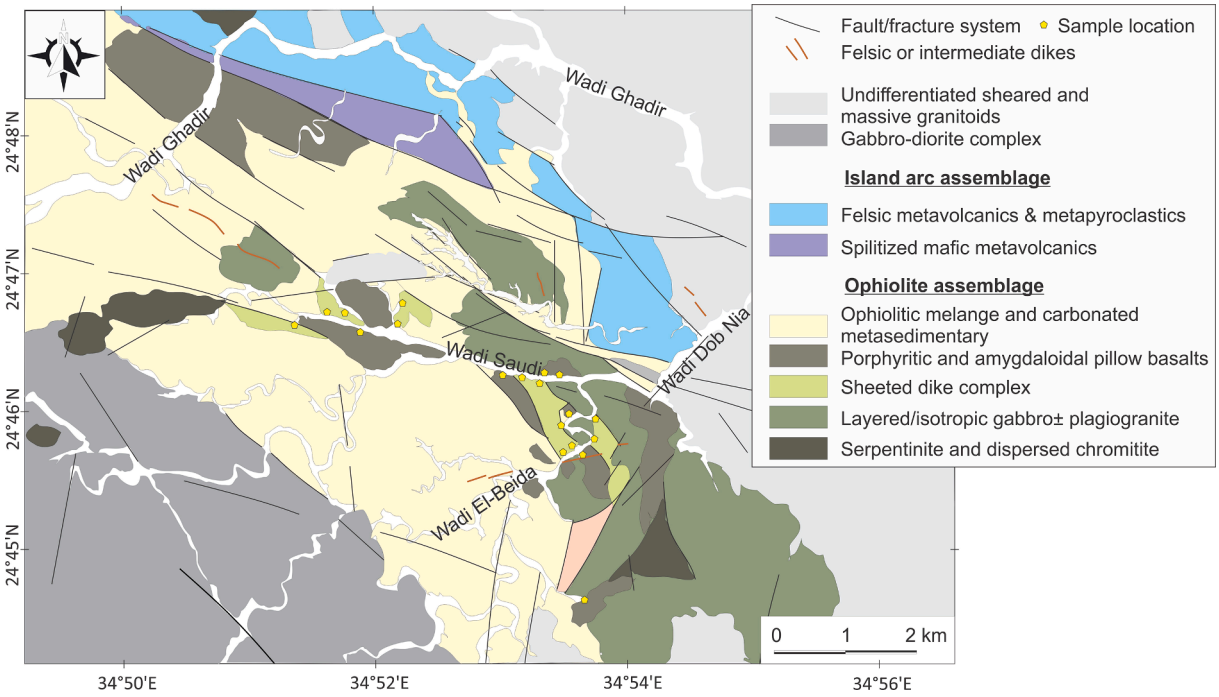

Fig. 2. Geological map of the Wadi Ghadir ophiolite, drafted by Basem Zoheir (this study) based on ASTER and Sentinel-2 data and verified by field data and numerous published maps (El Sharkawy and El Bayoumi, 1979; El-Bayoumi, 1980; Conoco Coral, 1987; EGSMA, 1997).

ophiolitic section at the Gabal Gerf area in the southern Eastern Desert. Abdel-Karim et al. (2016) suggested that features including fractionated LREE patterns and prominent Nb depletion in pyroxenite relicts and serpentinized peridotite from the Gabal Gerf ophiolite point to SSZ environment. Also, there is an enduring debate on the geodynamic setting of the ANS ophiolites. Many authors describe features of back-arc setting (e.g., El-Bayoumi, 1983; Furnes et al., 1996; El- Sayed et al., 1999; Farahat et al., 2004; Abd El-Rahman et al., 2009a; Basta et al., 2011), whereas others favor fore-arc basin setting for many of the ANS ophiolites (e.g., Ahmed et al., 2006; Ahmed, 2007; Azer and Stern, 2007; Khalil and Azer, 2007; Abd El-Rahman et al., 2009b; Ahmed, 2013). Mixed features of the two SSZ environments (i.e. forearc vs. backarc) for the Egyptian ophiolites have been documented by Abd El-Rahman et al. (2012), who identified two ophiolitic belts in the CED representing fossil arc–forearc and arc–backarc assemblages. Gamal El Dien et al. (2016) identified peridotites of different tectonic settings, including forearc, mid-ocean ridge and mid-ocean ridge-arc transition setting and concluded that this coexistence may reflect a transitional evolutionary history of the Neoproterozoic Mozambican oceanic lithosphere beneath the Eastern Desert. Based on new U-Pb zircon ages and Hf-O isotope data, Gamal El Dien et al. (2021) interpreted the Shadli bimodal and intermediate metavolcanic rocks in the South Eastern Desert as manifestations of mantle plume-induced reworking of MORB-like and arc-like oceanic lithosphere ~700 Ma.

Assessing the variation in the primary magma composition during the evolution of oceanic lithosphere would enable an updated geodynamic model for the Wadi Ghadir ophiolite. In the present work, we study the chemical variability in pillow lavas and sheeted dike complexes based on new whole-rock geochemical data and mineral chemistry analysis. In combination with the petrographic studies, the primary melts were calculated by hypothesizing hydrous melting conditions. The modeled primary melts were then used to determine the conditions of mantle melting and sequence of the tectono-magmatic processes. Thermodynamic modeling of the melt formation and evolution, constrained as pseudosections in the NCFMASTi chemical system, enables a better understanding of this important fragment of the Neoproterozoic oceanic crust, providing implications for the overall tectonic setting of the Arabian-Nubian Shield.

2. Geological setting and characteristics of Wadi Ghadir ophiolite

In the ANS, dismembered ophiolitic sections of generally Neoproterozoic ages form mountainous ridges or fragments of variable sizes tectonically incorporated in mélanges with carbonaceous and carbonated pelagic sediments. According to Stern et al. (2004) and Johnson et al. (2004), ophiolitic rocks in the ANS are scattered across most of the shield area, over a distance of ~3000 km (Fig. 1A). They occur as tectonized massifs, extensive mountainous ridges or continuous nappes, or intermingled with sedimentary and volcanic rocks in tectonic mélanges. Extensive ophiolite nappes are commonly associated with major suture zone that separate different tectonic terranes. As a result, most of the ophiolitic rocks are generally highly deformed and pervasively altered. Serpentinization and pervasive carbonation are observed in almost all occurrences of ophiolites in the ANS.

Dismembered ophiolitic sections form allochthonous nappes/belts and mélange terrains tectonically overlying island arc sequences or gneissic basement in the Egyptian Eastern Desert (Fig. 1B; Shackleton, 1994). Fig. 1B shows that the ophiolitic rocks form almost continuous belts across the central and southern sectors of the Eastern Desert, whereas exposures of these rocks are generally missing in the northern sector. Skackleton (1994) suggested that ophiolite sheets and mélanges, extending about 500 km north from the Onib-Sol Hamed suture, may represent rock association of a single back-arc basin. The original tectonic transport direction is hard to resolve, as protracted shortening and transcurrent fabrics overprinted deformed and locally obliterated the original subduction-related structures. A consensus exists, however, that the overall tectonic movement is dominated by west and NW-ward movement of the ANS towards the older craton west of the Nile (e.g., El Gaby, 1983; Abdelsalam et al., 2003 and references therein).

The Wadi Ghadir was the first recognized and comprehensively-studied ophiolitic section in the Nubian shield (El Sharkawy and El Bayoumi, 1979; El-Bayoumi, 1980; Kröner et al., 1992). The most intact sequence occurs in the Wadi El-Beda and Wadi Saudi areas, where

Fig. 3. Field relationships of the ophiolitic rocks in Wadi Ghadir area. (A) Serpentinized peridotite tectonites at Gabal Lawi, (B) Preserved peridotite block embedded in carbonated siltstone-dominated ophiolitic mélange matrix, (C) Layered gabbro exposure at the conjunction of Wadi Dob Nia and Wadi El-Beda, (D) Pegmatitic, isotropic gabbro at Wadi Saudi, (E) Sheeted dike complex cutting metagabbros at the Wadi El-Beda entrance, (F) Sheeted dikes block in the ophiolitic mélange at the western part of Wadi Saudi, (G) Discrete dikes cutting serpentinized ultramafic blocks in the ophiolitic mélange matrix, (H) An outcrop of pillow lavas at the Wadi Saudi area. Notice the cross-cutting dike with nearly the same composition (andesitic basalt), (I) A close up view of the pillow lava at Wadi El-Beda.

layered gabbro, pillow lava and sheeted dike complex are exposed (Fig. 2). Ophiolitic rocks in the Wadi Ghadir area include serpentinized peridotites, gabbro complex, sheeted dikes, and pillow lavas. A thin layer of deep-sea sediments and metasiltstones is admixed with the intensely tectonized ophiolitic matrix in most exposures. Serpentinite forms large mountainous masses west of the study area, or occurs as massive and schistose bodies cross-cut by listvenite veins. Less abundant intact peridotites are locally observed in the mélange (Fig. 3A, B). In addition to the ophiolitic rocks, Wadi Ghadir ophiolitic mélange comprises blocks of thin stratified volcaniclastic rocks, debris of laminated argillite, greywacke, marble, metagabbro, quartzite, chert, muscovite and tuffaceous metavolcanic rocks (e.g., El Sharkawy and El Bayoumi, 1979; El-Bayoumi, 1983; Farahat et al., 2004).

The gabbro complex constitutes an important component of the Wadi Ghadir ophiolite. Three varieties are observed in the study area, including layered, isotropic, and hypabyssal gabbros (El-Bayoumi, 1980; Kröner et al., 1992; Abd El-Rahman et al., 2009a,b). The layered gabbro is the most important and distinctive component of the complex. It is exposed at the conjunction of Wadi Saudi and Wadi Dob Nia, a tributary of the main Wadi Ghadir (Fig. 2). At the exposure scale, rhythmic mesocratic-melanocratic layering grades upward into an isotropic gabbro variety and is overlain by hypabyssal gabbro (Fig. 3C, D). The alternating layers comprise pyroxenes, plagioclase, opaque minerals, and apatite. Subordinate serpentine, talc, garnet, tremolite and anthophyllite are observed in some samples. The isotropic gabbro variety occurs as a coarse- to medium-grained rock, composed essentially of clinopyroxene, plagioclase, hornblende, chlorite, and apatite. Calcite and serpentine are secondary minerals. Pyroxenes include augite and less common hypersthene. Plagioclase (An_{50-70}) occurs as tabular and elongate crystals, locally altered into epidote and kaolinite. Hornblende forms short prismatic crystals, replaced in part by chlorite. The studied gabbro samples show phaneritic, granoblastic, and less common ophitic textures (Fig. 3D). The hypabyssal gabbro variety is composed mainly of plagioclase, hypersthene, diopside, and hornblende, whereas apatite, garnet, and iron oxides are accessory minerals. Uralitic amphibole and relict olivine are altered into talc and iron oxides. Small (a few meters-across) irregular pods of pegmatitic gabbro and vein-like bodies of plagiogranite occur in the fresh exposures along Wadi Saudi.

The volcanic rocks of the Wadi Ghadir ophiolite comprise pillow lavas and several dike complexes. These dikes are diabase (andesitic) and basaltic in composition. Based on the field relationships, the Wadi Ghadir dike complexes can be categorized into three groups: sheeted dikes type-I that occur as scattered blocks typically with asymmetric chilled margins and are incorporated in the ophiolitic mélange (Fig. 3E). These dikes were observed in the western part of the Wadi Saudi area (Fig. 3E). Sheeted dikes type-II are associated with or cut layered gabbros and pillow lavas along Wadi El-Beda and Wadi Saudi. These dikes vary significantly in width from a few cm up to 4 m (Fig. 3F). Discrete individual dikes cut the gabbroic and pillow lava section, and exhibit deformation features conformable to that of their host rocks. These dikes are not sheeted and are mainly andesite in composition. Locally, these

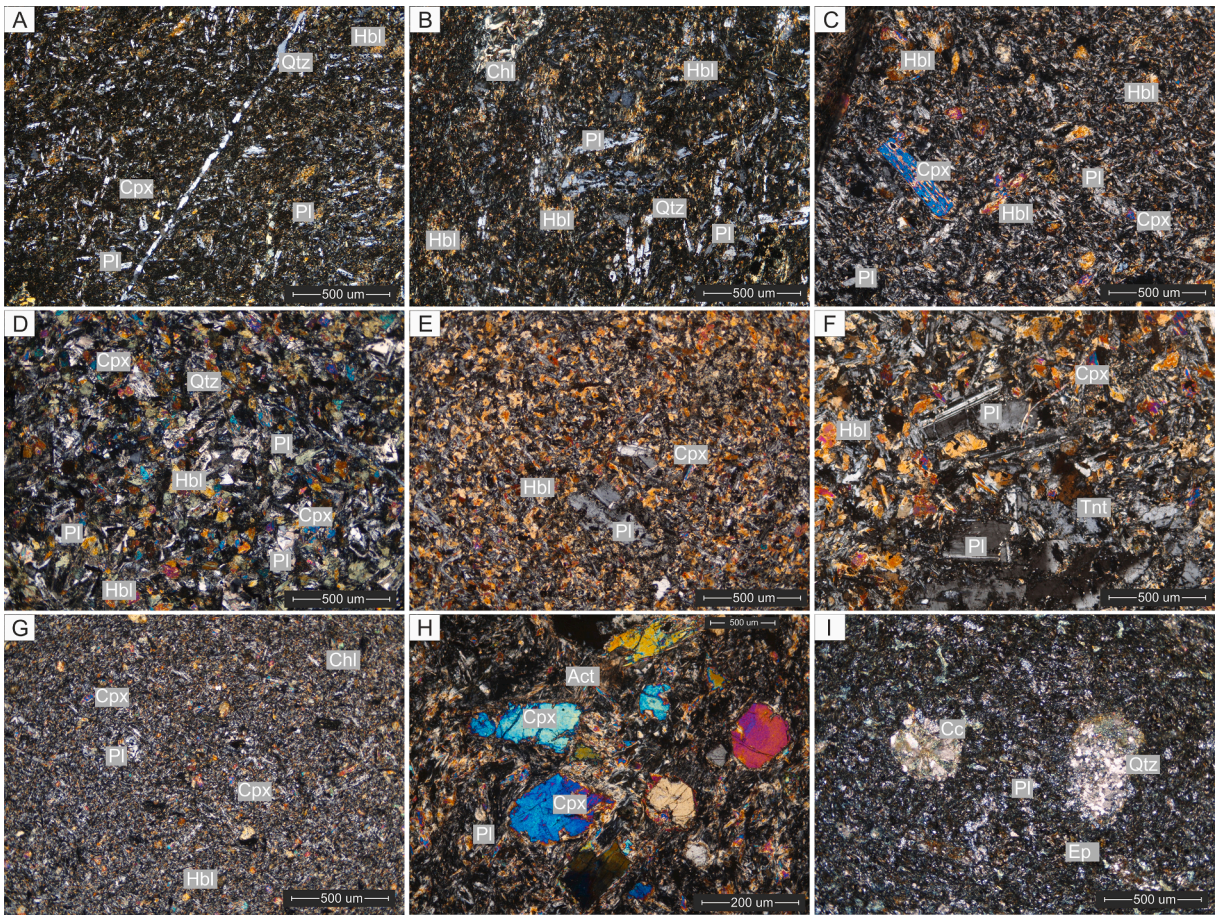

Fig 4. Photomicrographs (XPL) of the volcanic rocks of the Wadi Ghadir ophiolite: (A) Sheeted dike (type-I) sample showing fealty-textured microcrystalline groundmass of plagioclase (Pl), clinopyroxene (Cpx) and iron oxides. Microphenocrysts of hornblende (Hbl) and clinopyroxene are conspicuous and a late thin quartz (Qtz) veinlet dissects the texture, (B) Sheeted dike (type-I) sample showing long prismatic, sub-trachytoid aligned plagioclase crystals embedded in a fine granular mosaic of plagioclase, clinopyroxene and iron oxides, (C) Sheeted porphyritic diabase dike (type-II) with long prismatic augite microphenocryst in a fine-grained microcrystalline mesostasis of plagioclase, pyroxene, rare quartz, and accessory iron oxides, (D) Sheeted doleritic dike (type-II) sample showing interlocking granular/interstitial and sub-ophitic textures of relatively fresh clinopyroxene, plagioclase, and hornblende. Some plagioclase microlites exhibit quenched morphologies. Also seen is a thin veinlet of quartz, (E) Discrete basaltic andesitic dike showing a porphyritic texture with large plagioclase phenocrysts and abundant hornblende and plagioclase in the groundmass. Clinopyroxene microphenocyrsts are uncommon and iron oxides are accessory minerals, (F) Discrete andesitic dike with large prismatic plagioclase phenocrysts and less common clinopyroxene in a medium grained groundmass. Titanite (Tnt) is accessory mineral, (G) A pillow lava sample with intergranular and porphyritic textures with relatively fresh clinopyroxene microphenocrysts and plagioclase. Chlorite (Chl) replaces clinopyroxene and quartz is rare, (H) Porphyritic pillow lava sample with subhedral clinopyroxene and plagioclase phenocrysts. Some microphenocrysts have irregular/corroded boundaries and locally quenched morphologies. Plagioclase and actinolite (Act) in the groundmass occurs as fibrous laths wrapped around the clinopyroxene phencrysts, (I) A pillow lava sample showing poorly developed flow texture with local microcrystalline silica spots showing a tailed morphology. Plagioclase microphenocrysts are saussuritised and are partially replaced by epidote (Ep). Two rounded amygdules stuffed with microcrystalline silica and calcite (Cc).

dikes are gently dipping or forming sill-like structure in the altered host rocks (Fig. 3G). These discrete dikes represent a distinctive group of the dike complexes in the Wadi Ghadir ophiolite. Towards the west of the study area, Abd El-Wahed et al. (2019) reported irregular and gradual contacts between sheeted and discrete dike complexes and the overlying pillow lava section along Wadi Lawi. Pillow lavas form large blocky exposures and still preserve their pillowed morphology (Fig. 3H, I). In the Wadi Saudi are, deformed pillows are cut by discrete dikes that show no chilled margins.

The sheeted dikes type-I are mainly andesitic basalt in composition with ubiquitous porphyritic and trachytoidal texture (Fig. 4A, B). Clinopyroxene phenocrysts are partially replaced by chlorite. Plagioclase laths and hornblende are fairly fresh. Rare anhedral and interstitial quartz is observed in some samples. The sheeted dikes type-II are diabase with long-prismatic clinopyroxene and subhedral plagioclase microphenocrysts in a pyroxene-hornblende-iron oxides groundmass (Fig. 4C, D). Small irregular quartz grains are commonly associated with hornblende. The discrete dikes are composed of hornblende, plagioclase and less abundant clinopyroxene. Large plagioclase phenocrysts are embedded in a granular hornblende-plagioclase groundmass. Titanite is accessory and is commonly associated with hornblende (Fig. 4E, F).

Pillow lava samples are intergranular and subophitic rocks that are composed mainly of plagioclase, clinopyroxene, and less common actinolitic hornblende (Fig. 4G, H). Plagioclase is locally replaced by saussurite and epidote, whereas clinopyroxene is replaced by chlorite ± uralite. Titanite and iron oxides are accessory minerals. Abd El-Rahman et al. (2009) suggested that the pillow lavas cropping out in the Wadi Saudi area differ from the pillows of the Wadi El-Beda in terms of texture and geochemical composition. We, however, did not identify textural differences during the field work or microscopic investigation. Pillow lava samples showing pronounced spilitization and replacement by calcite were excluded from the geochemical analysis. The reason is the advocated substantial mobility of most of the high-field-strength (HFS) elements, i.e., Ti, Y, P, Zr, and Nb, during greenschist facies metamorphism (Murphy and Hynes, 1986).

Porphyritic and vesicular textures are observed in the same samples

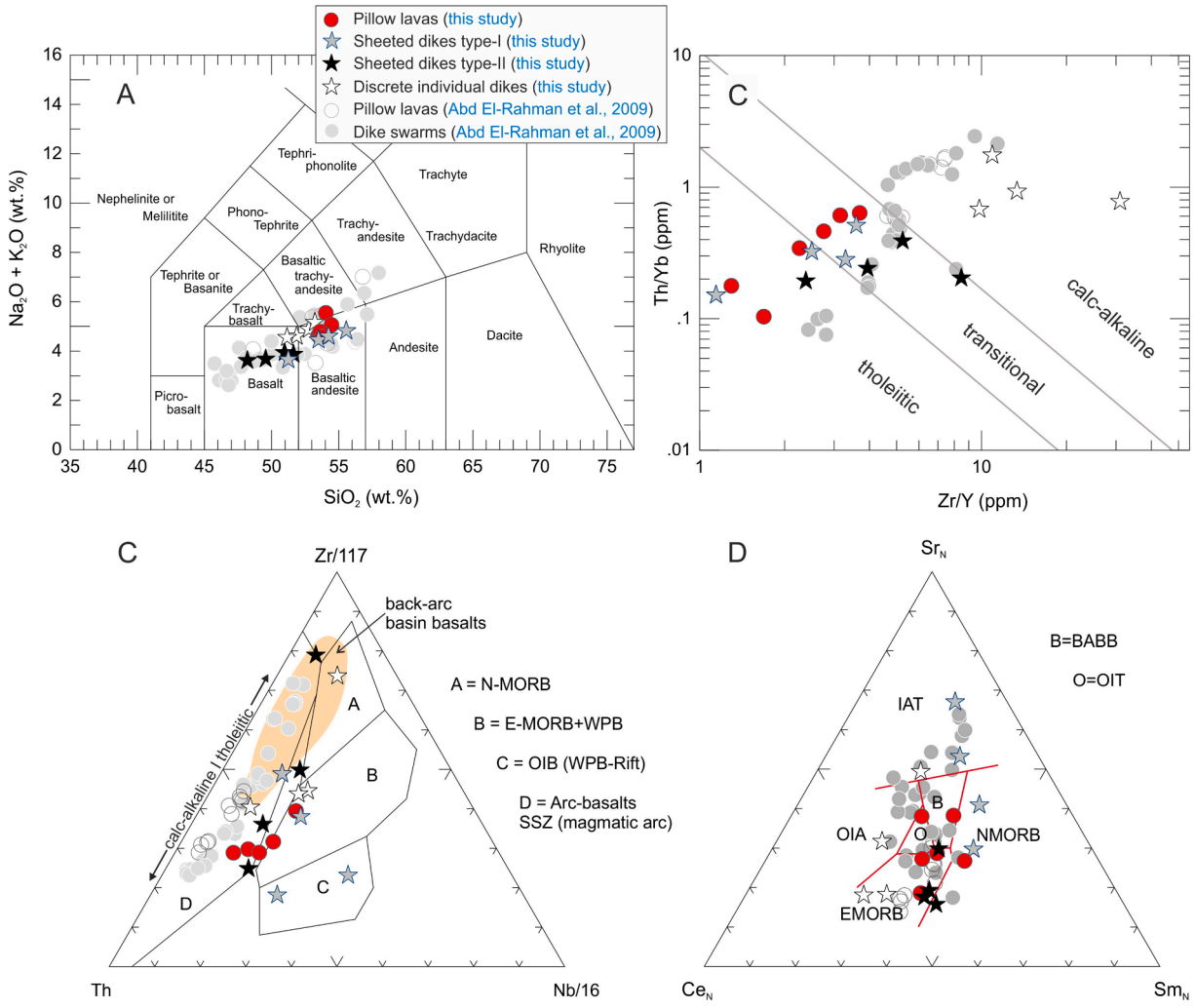

Fig. 5. Igneous rock classification diagrams using (A) SiO_2 vs. total alkalis (Le Maitre, 1989). The mafic volcanic rocks of the Wadi Ghadir ophiolite are mostly subalkaline and basaltic to andesitic in composition. Also shown are data of well-described volcanic rocks from the Wadi Ghadir ophiolite (Abd El-Rahman et al., 2009a,b), (B) Discrimination of magma series by trace element data following the method of Ross and Bedard (2009). In Zr/Y – Th/Yb space, the studied ophiolitic rocks spread from tholeiitic through transitional to calc-alkaline series, (C) Th-Zr/117-Nb/16 discrimination diagram (Wood, 1980) with data of the investigated ophiolitic volcanics. A.N-MORB type; B. E-MORB type and tholeiitic basalt within plate and differentiates; C. alkaline within plate basalt and within plate basalts and differentiates; D. convergent plate-margin basalts and differentiates (subduction zone). The field of back-arc basalts is from Metzger et al. (2002), (D) Ce_N-Sr_N-Sm_N diagram of Ikeda (1990), concentrations are normalized to primordial mantle composition (Ce 1.9 ppm, Sm = 0.385 ppm and Sr = 23 ppm). IAT (island arc tholeiite), BABB (back-arc basin basalt), N-MORB (normal MORB), E-MORB (enriched MORB), OIT (ocean island tholeiite) and OIA (ocean island alkalic basalt).

collected from Wadi Saudi area. The original morphologies are relatively well preserved, but some pillows are strongly deformed. Some well-preserved pillows exhibit oval or elliptical to circular morphologies, with massive cores and vesicle-rich marginal domains. In thin sections, cores of these pillows are mainly aphyric basalt and porphyritic in places (Fig. 4H). The mineral composition includes plagioclase (An_{60-80}), clinopyroxene, and chlorite. Apatite and iron oxides are accessory minerals. Phenocrysts of pyroxenes and amphibole set in a cryptocrystalline groundmass of altered plagioclase, chlorite, epidote and iron oxides. The marginal domains are characterized by a distinct amygdaloidal texture, partially filled by microcrystalline quartz and calcite (Fig. 4I).

3. Analytical methods

3.1. Whole-rock geochemistry

Whole-rock geochemical analysis was carried out on a set of petrographically-characterized samples of the ophiolitic volcanic rocks from Wadi Ghadir, Wadi El Beda, and Wadi Saudi areas. The loss on ignition (LOI) values were determined by heating the rock powder in a vacuumed oven at 1000 °C for 1 hr on samples dried for 3–4 hr at 110 °C. Major element composition by X-ray fluorescence spectrometry (XRF) on fused pellets using a Magix Pro PW 2540 XRF was carried out at the Institute of Mineralogy and Petrology, the University of Hamburg (Germany). International reference standards (JA-3, JB-2, JB-3, JGB-1, and JG-3) were used for calibration.

From each sample, ~100 mg of the whole rock powder was digested in concentrated HF-HNO_3, followed by concentrated HNO_3 and then dried. The dried samples were re-dissolved and diluted in 2% ultrapure HNO_3 and subsequently analyzed by inductively coupled plasma mass spectrometry (ICP-MS) on a Thermo iCapQc™ mass spectrometer at Rutgers University (USA). Three standards (BCR-2, BIR-1a, and BHVO-2) were used to calibrate the instrument with regressions yielding r^2 values of at least 0.99 for all of the elements measured. Each sample analysis consisted of 10 main runs, with each run containing 10 sweeps of the desired mass range. An acid blank and calibration standards were analyzed every 15 samples to ensure instrument calibration. The

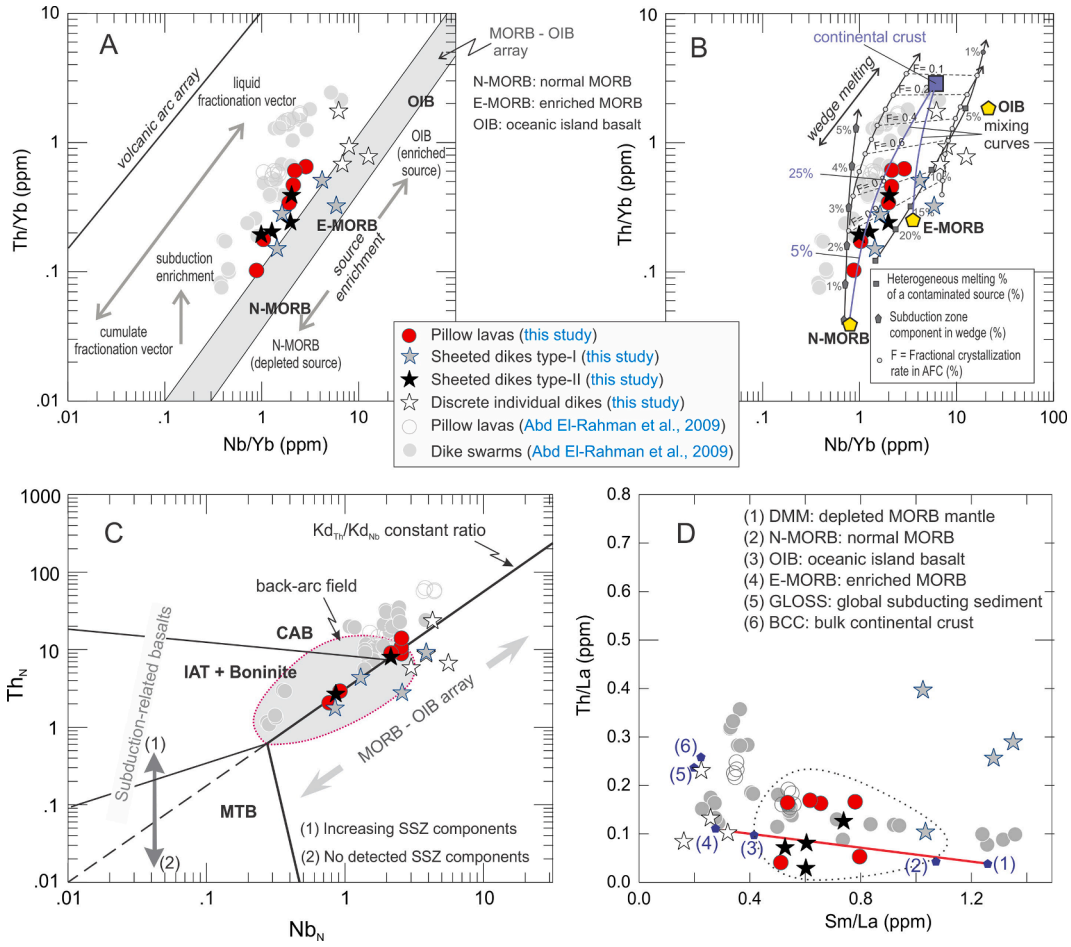

Fig. 6. (A) Th/Yb vs. Nb/Yb diagram with data of the Wadi Ghadir ophiolitic volcanic rocks plotted relative to the MORB-OIB and volcanic arc arrays as defined by Pearce (2008). N-MORB, E-MORB, and OIB are from Sun and McDonough (1989), (B) Same as (A) with data points plotted relative to the different petrogenetic modeling by Pearce (2008). The modeled trend AFC (assimilation-fractional crystallization trajectories), in which enriched and depleted magmas are interacted are from De Paolo (1981). Average continental crust is from Albarède (2003). The two lines illustrate mixing of continental crust with N-MORM and E-MORB, (C) N-MORB-normalized Th versus Nb diagram (Saccani et al., 2018) for volcanic rocks from the Wadi Ghadir ophiolite. Normalizing values are from Sun and McDonough (1989). MTB: medium-Ti basalt; IAT: island arc tholeiitic basalt (low-Ti); CAB: calc-alkaline basalt; SSZ: suprasubduction zone. Vectors indicate the trends of compositional variations due to the main petrogenetic processes, (D) Th/La vs. Sm/La plot for the Wadi Ghadir ophiolitic basalts and dolerites (after Plank, 2005). Most of the samples plot along the mixing lines between DMM (depleted MORB mantle source) and E-MORB, similar to the back-arc basin basalts (e.g., Fretzdorff et al., 2002). The spread away from this mixing line upwards is related to variable Th/La enrichments, typical for basalts from enriched mantle sources additionally fluxed with variable amounts of crustal material or melts from subducted sediments. Values for N-MORB, OIB and E-MORB are from Sun and McDonough (1989), DMM from Workman and Hart (2005), BCC from Rudnick and Gao (2003), and GLOSS from Plank and Langmuir (1998). The 'broken line' field contains 70% of the samples and suggests similar geochemical affinities for the pillow lavas and sheeted dikes type-II.

instrument calibration was also monitored by measuring the international reference standards, as well as the internal standards run as unknowns.

3.2. *Mineral chemistry*

Petrographic investigations were aided by SEM back-scattered electron imaging. The chemical composition of clinopyroxene phenocrysts in least-altered samples was determined using a CAMECA SX50 electron probe microanalyzer (EPMA) at the Technical University of Clausthal (TU-Clausthal, Germany). The microanalyzer is equipped with five wavelength-dispersive goniometers and an energy-dispersive spectrometer. Operating conditions were 15 kV accelerating voltage and 15 nA beam current. Beam diameter was 1–5 μm, depending on the occurrence of mineral inclusions, and the counting time was 20 s. Natural silicate, oxide, and free element standards were used for calibration.

Trace element composition of clinopyroxene phenocrysts were performed at the University of Kiel, using a 193 nm ArF excimer laser ablation system (GeoLasPro Plus, Coherent) coupled to an Agilent 7500 s ICP-MS. The samples were loaded into a Zurich-type low dispersion high capacity laser ablation cell flushed with 1.0 L/min He as the carrier gas. Addition of 14 mL/min H_2 into the He carrier gas stream before entering the ablation cell led to an increase in sensitivity and reduction of oxide formation. The laser was set to a pulse frequency of 5 Hz and pulse energy of 2.6 J/cm^2 on the sample surface with a 50 μm spot size. The laser was automatically switched on for 60 s for signal acquisition and then off for 20 s for background levels to be attained and measured. To reduce the potential error from surface contamination, the first 5–10 s of each sample acquisition were discarded from data integration. The GLITTER software package (Griffin et al., 2008) was used for data reduction using the graphical visualization tool for setting integration intervals for each analyzed spot. GLITTER external calibration was done with silicate glass NIST SRM612 using ^{48}Ca for internal standardization.

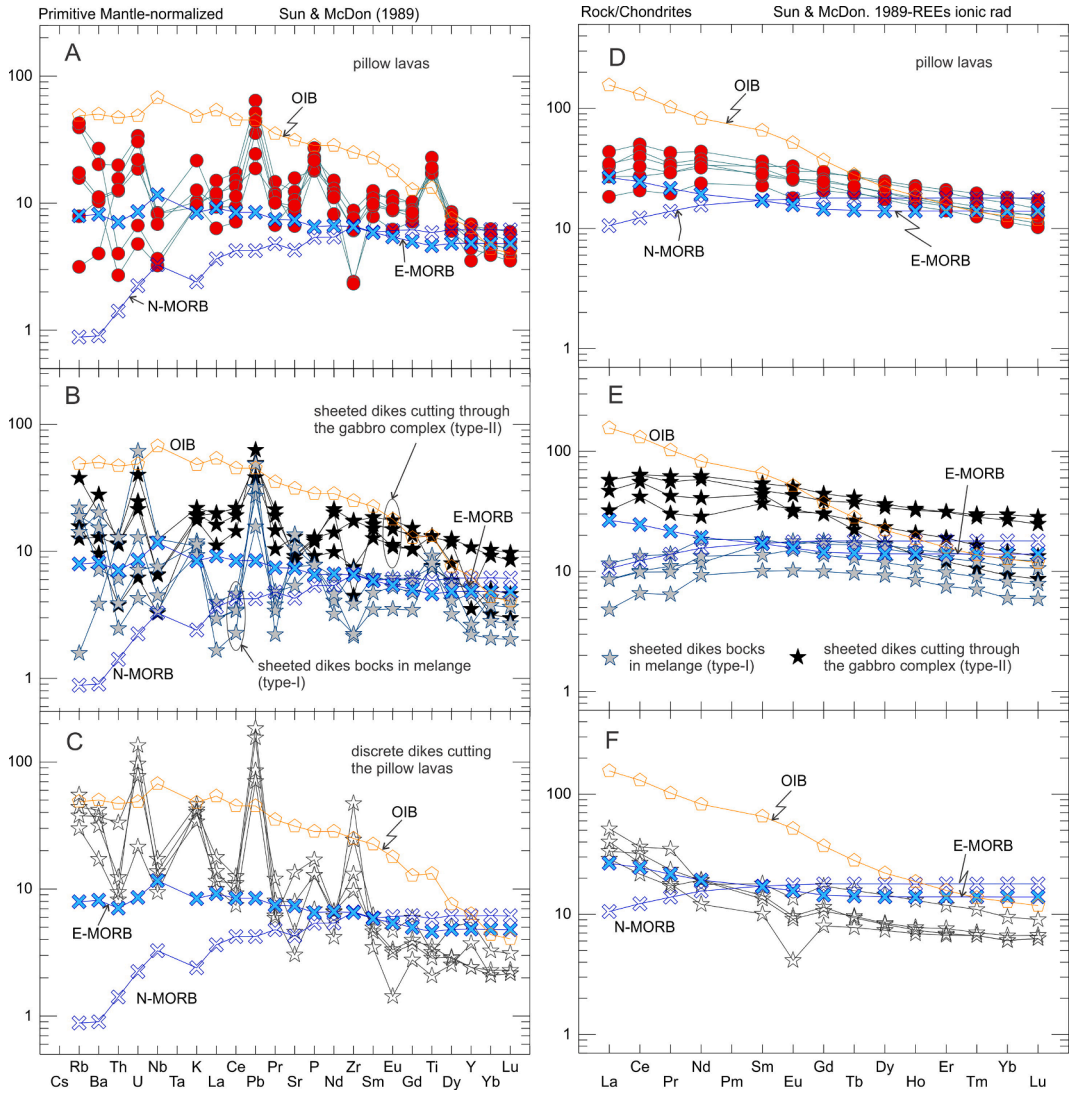

Fig. 7. Primitive mantle-normalized trace element patterns of the pillow lavas (A), sheeted dikes (B) and crosscutting dike sets (C). Also shown are patterns for N-MORB, E-MORB and OIB based on reference values from Sun and McDonough (1989), (D)–(F) Chondrite-normalized REE patterns of the same rock sets. Gray hatched fields in F represent data of D4 dikes of Abd El-Rahman et al. (2009) are given for comparison.

4. Geochemistry

4.1. Whole-rock geochemistry

Whole-rock geochemical data of 6 pillow lava samples, 8 sheeted dikes samples, and 4 samples of the discrete dikes are listed in Supplementary Table 1. The data reveal that the studied rocks show distinctly different Mg# values (Mg# = 100 × Mg/[Mg + Fe^t]), 28–37 for the pillow lavas and 49–63 for the different dike complex types, suggesting variable degrees of fractional crystallization (Tatsumi and Ishizaka, 1982). The limited variation in the elemental distribution in each group of the studied rocks combined with the relatively low percentage of the loss-on ignition (Supplementary Table 1) are taken as evidence of slight alteration.

The total alkalis-silica classification scheme (Le Maitre et al., 1989) depicts a continuous array from basalts through basaltic andesites to trachyandesites (Fig. 5A), implying that alkalis and silica contents in these rocks remained almost unchanged by greenschist metamorphism. The lithogeochemical characteristics of the investigated rocks are based on trace elements such as Ti, Zr, Hf, Yb, and Nb, and the REE, which have been considered to be least susceptible to alteration and fairly immobile during greenschist facies metamorphism (e.g., Pearce and Wyman, 1996).

Variations in some immobile trace elements and their ratios, i.e., Zr/Y, La/Yb, and Th/Yb, are commonly used to assess the original magmatic affinities (e.g., Jenner, 1996; Pearce and Wyman, 1996). The trace element composition of the Wadi Ghadir ophiolitic volcanic rocks reflects a wide spectrum from tholeiitic through transitional to calc-alkaline series (Ross and Bédard 2009; Fig. 5B). According to Beccaluva and Serri (1988), Yb and Dy concentrations in oceanic basalts account for different degrees of partial melting and/or depletion of the mantle sources. With the exception of four boninite-like samples (discrete dikes that cut the pillow lava), all samples analyzed for this study as well as all geochemical data in Abd El-Rahman et al. (2009) show IAT affinities and define an array at high angle to the discriminant boundary, consistent with an early stage of island arc development (e.g., Beccaluva and Serri, 1988).

Based on the widely used Th-Zr-Nb discrimination diagram of Wood (1980), the ophiolitic rocks display features typical of E-MORB and overlap the field of basalts with subduction signatures (Fig. 5C). Limited disturbance of this scheme might have been caused by early crystallization and separation of zircon (e.g., Reagan and Meijer, 1984), which may explain the two samples that are outliers compared to the majority of the other compositions. In the primordial mantle-normalized Ce-Sr-

Sm plot of Ikeda (1990), the studied rocks scatter in most fields, but define an evolutionary trend from E-MORB to IAT compositions (Fig. 5D). Petrogenetic trace element ratios such as Th/Yb, Nb/Yb, and Zr/Nb indicate that the Wadi Ghadir ophiolitic volcanic rocks have subduction-modified E-MORB chemistry (e.g., Pearce, 2008).

The majority of sheeted dikes and pillow lava samples for this study together with all data of Abd El-Rahman et al. (2009) spread between the N-MORB and arc basalts reference composition. All data points consistently define a typical subduction trend from the MORB-OIB oceanic array to the volcanic arc array (Fig. 6A). The range of Th/Yb values possibly reflect various degrees of siliceous melt/fluid contamination of the mantle source in a subduction environment (e.g., Saunders et al., 1988; Pearce and Peate, 1995; Pearce, 2008). Petrogenetic modeling of the studied rocks based on the Pearce (2008) diagram (Fig. 6B) indicates that the magma compositional trend was a result of different amounts (1% to >5%) of subduction component input into a depleted mantle source. This contaminated mantle source was subjected to heterogeneous partial melting (from 5% to >20%) and experienced variable but generally high rates of assimilation-fractional crystallization (AFC = up to 0.9). It also shows that the pillow lava and sheeted dikes have had a common evolution history with ≲25% contaminated continental components, whereas the discrete dikes had a noticeably different evolution path.

Th and Nb values are ~1–10 times N-MORB composition, and overlap those of IAT, boninitic and calc-alkaline basalts (Saccani, 2015). Our data, together with data reported by Abd El-Rahman et al. (2009), show variable Th enrichment with respect to Nb. The data points straddle the line delineating Th enrichment relative to Nb (enrichment-depletion array; Fig. 6C), reflecting variable subduction-related contributions in the source magmas of the studied rocks (cf. Saccani et al., 2018). Fig. 6C shows that most volcanic rocks plot in the field of back-arc basin basalts (BABB) with or without input of subduction or crustal components (Saccani, 2015).

Th/La vs. Sm/La diagram of Plank (2005) detects sediment recycling at subduction zones and estimates mantle-sediment mixing extent (Fig. 6D). The data show variable Th/La (0.03–0.40) and Sm/La ratios (0.16–1.35) similar to those of back-arc basin/rift basalts with heterogeneous additions from enriched MORB to depleted mantle source (e.g., DMM). The scatter of several samples away from the binary DMM – E-MORB mixing line is a feature of many OIB and MORB basalt suites, and emphasizes variable contributions from exotic components (e.g., Thirlwall et al., 2004).

The primitive mantle-normalized multi-element diagrams (Fig. 7A–C) reveal that these rocks are generally enriched in almost all elements compared to the reference N-MORB. These rocks also exhibit slight negative Nb anomalies, and depletions in Y, Yb and Lu compared to the typical E-MORB trend. The variable enrichments in large-ion lithophile elements (LILE) such as Pb, Rb, K, Cs, U and Th ($[Th/La]_N$ = 0.23–3.2) relative to high field strength elements (HFSE) such as Ti, Nb, and Y are typical characteristics of subduction-related magmas (Kelemen et al., 1993; Rolland et al., 2000). Zr is considerably enriched in the late dikes (dikes that cut the pillow lavas), but it shows mixed behavior in the pillow lavas and other dike types. Noteworthy, the pillow lavas and sheeted dikes have $[Nb/La]_N$ ratios of 0.2–0.9 distinguishing them from dikes crosscutting the gabbro complex and pillow lavas ($[Nb/La]_N$ = 0.8–4.6).

The chondrite-normalized REE patterns of the pillow lavas are mildly enriched in LREE relative to HREE (Fig. 7D; $[La/Yb]_N$ 1.4–3.1), intermediate between the E-MORB and OIB, and are noticeably distinct from the N-MORB (Fig. 7D). The dike complexes have distinct REE patterns, with variable LREE enrichments ($[La/Yb]_N$ averages of 0.9, 2.8 and 5.4; Fig. 7E, F). The chondrite-normalized REE patterns of the discrete dikes that crosscut the pillow lavas are characterized by enriched LREE, and generally depleted HREE relative to N-MORB and E-MORB (Fig. 7E, F), typical of calc-alkaline magma series. Moderate or mild negative Eu anomalies characterize these late dikes (Eu/Eu* = 0.5 – 0.8) compared

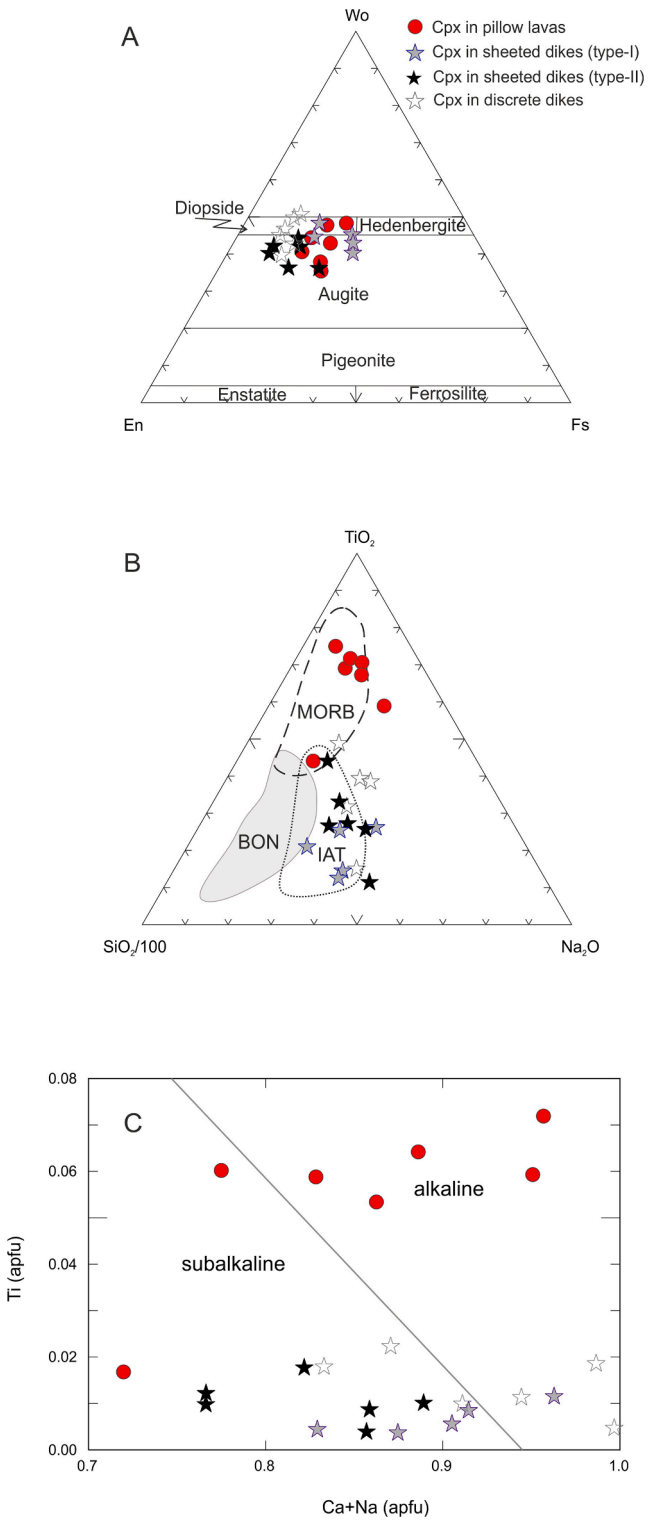

Fig. 8. (A) Wo-En-Fs classification diagram of Morimoto (1988) with data of Cpx from the Wadi Ghadir ophiolitic volcanic rocks, (B) $SiO_2/100$–TiO_2–Na_2O (wt.%) for discrimination of clinopyroxene in the Wadi Ghadir ophiolitic volcanic rocks (Beccaluva and Serri, 1988), (C) Ti vs. Ca + Na (Leterrier et al., 1982) diagram for the Wadi Ghadir ophiolite. MORB, Mid-ocean ridge basalt; OIB, Ocean-island basalt and BABB, Back-arc basin basalt.

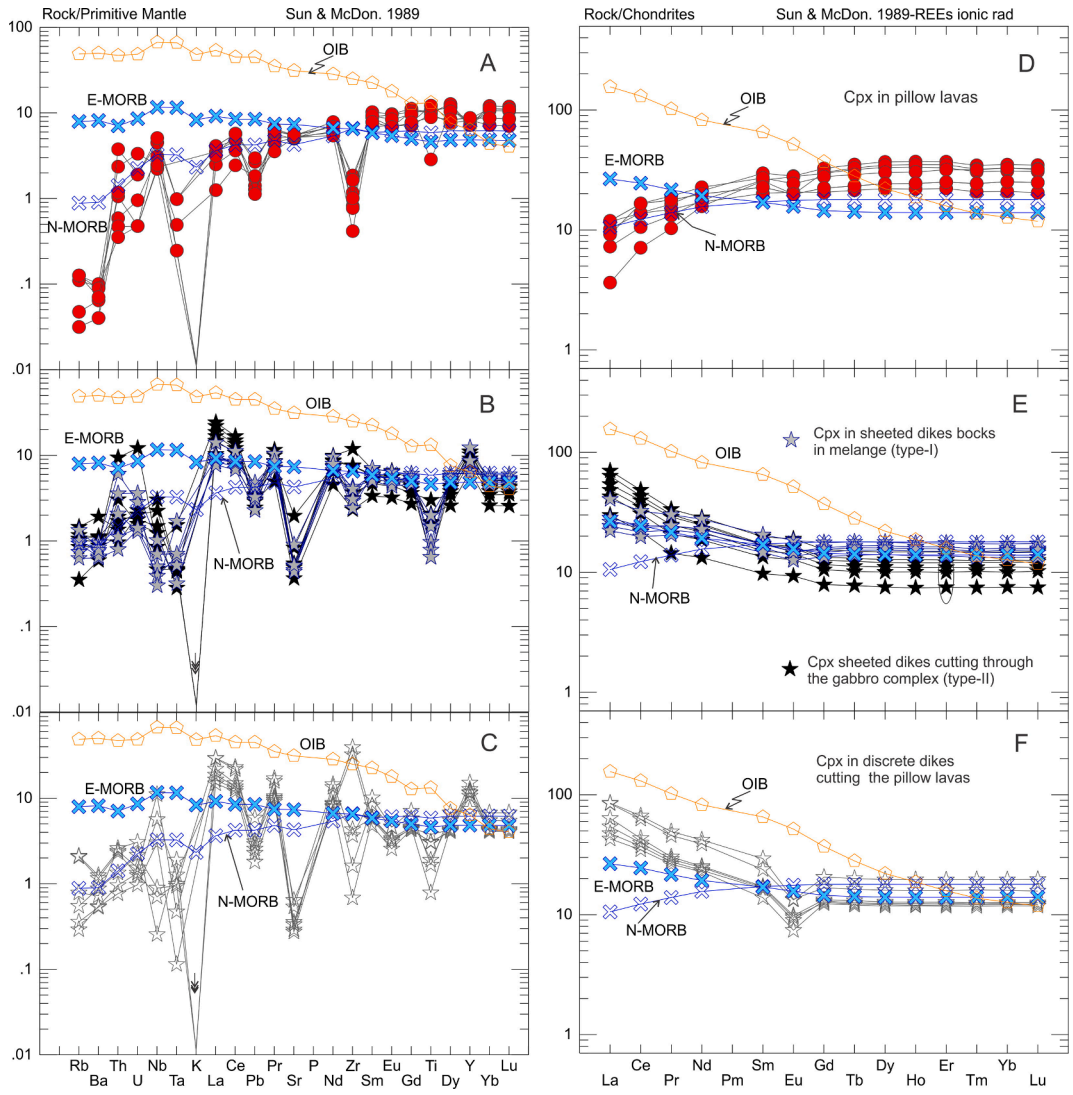

Fig. 9. Primitive mantle-normalized trace element patterns of Cpx from pillow lavas (A), sheeted dikes (B) and discrete dikes in pillows (C). Also shown are patterns for N-MORB, E-MORB and OIB based on reference values from Sun and McDonough (1989), (D)–(F) Chondrite-normalized REE patterns of the same rock sets. Normalization values are from Sun and McDonough (1989).

to very weak or no anomalies in other volcanic rocks from the Wadi Ghadir ophiolite (Eu/Eu* = 0.8–1.1) (Fig. 7D–F).

4.2. *Clinopyroxene composition*

EPMA data and calculated structural formulae of clinopyroxene (Cpx) phenocrysts in the investigated samples are listed in Supplementary Table 2. The data reveal variable contents of Al_2O_3 (2.72–9.71 wt %), Cr_2O_3 (0.1–1.61 wt%), FeO (4.78–10.16 wt%), MgO (8.77–15.77 wt %), CaO (18.18–24.18 wt%), MnO (0.16–0.69 wt%), Na_2O (0.23–0.97 wt%) and TiO_2 (0.14–2.64 wt%). Cpx in the pillow lava samples is distinctly Ti-rich with Ti/Al ratios are mostly > 0.25, whereas Cpx chemistry of the dike complexes displays significantly low Ti/Al ratios (0.02–0.13), likely implying different degrees of mantle source depletion (Pearce and Norry, 1979).

The analyzed Cpx grains span a wide compositional range (Wo = 39–57), and some analyses plot above the "Wo = 50%" line (Morimoto, 1988). Thus correction of the high contents of Ca-Al-Tschermak's and Ca-Ti-Tschermak's molecules was done by applying the algebraic model of Dietrich and Petrakakis (1986). Using the WinPyrox program (Yavuz, 2013), the corrected values of end-members, e.g., Wo-En-Fs, Q-Jd-Aeg, Wo-Hyp-Jd, and Aug-Jd-Aeg in%, are calculated using the simple formula compiled by Soto and Soto (1995). Classification of the studied Cpx by employing the WinPyrox (Yavuz, 2013) and by plotting the corrected end members (i.e., Wo = 29.3–41.7) on the diagram of Morimoto (1988) consistently indicate that these Cpx are diopside and augite (Fig. 8A).

The structural formula calculations show low Fe^{3+} (≤0.09 apfu) in Cpx from the crosscutting dike samples. This considerable variation reflects changes in the oxygen fugacity conditions. Beccaluva and Serri (1988) suggested that high-Ti ophiolites are typical of the MORB and back-arc basins, whereas low-Ti and very low-Ti ophiolites are best equated with the island arc and fore-arc (boninitic) environments, respectively, produced in the supra-subduction zone settings (e.g., Parlak et al., 2002). The Wadi Ghadir sheeted and discrete dike complexes plot exclusively in the island arc tholeiite field (Fig. 8B). Clinopyroxenes from the Wadi Ghadir volcanics have transitional compositions from subalkaline to alkaline (Fig. 8C; Leterrier et al., 1982), which is consistent with a transitional subduction to intraplate environment (e.g., Loucks, 1990).

Pressure estimates for the analyzed clinopyroxenes, based on the single pyroxene geobarometer of Nimis and Ulmer (1998), reveal distinctly different pressure conditions for the pillow lava and dike complexes (see Supplementary Table 2). The advantage of the Nimis and

Ulmer (1998)'s barometer is that it is independent of temperature conditions. Variations of major elements in the melt for basalts with normal contents of Al_2O_3 (<18 wt%) do not reduce the accuracy of the geobarometer (Nimis, 1995). However, the single-clinopyroxene barometer has a tendency to progressively underestimate pressure at P > 4.5 GPa (e.g., Ziberna et al., 2016), particularly for melts with >1% H_2O. Consequently, we favored the Putirka (2008) Jd-in-clinopyroxene barometer, where WinPyrox (Yavuz, 2013) successfully solves the dataset iteratively with equation 32 of Putirka (2008). The results indicate mean pressure conditions (in kbar) for the pillow lavas, sheeted dikes type-I, sheeted dikes type-II, and discrete dikes are 8.6 ± 2.2 (1σ), 11.3 ± 1.3 (1σ), 12.1 ± 0.7 (1σ), 12 ± 0.6 (1σ) (Supplementary Table 2).

The enstatite-in-Cpx thermometer of Nimis and Taylor (2000) is known to have limitations concerning its reliability and applicability (e.g., Cookenboo and Grütter, 2010). Low-quality microprobe data were highlighted as resposnsible for unreliable clinopyroxene thermobarometry outcomes (e.g., Mather et al. 2011). On the other hand, the Putirka (2008) model is considered the most precise clinopyroxene-liquid thermometer. Putirka (2008)' thermometers and barometers can be used to calculate *T* and *P* to a precision of ±30 °C and ±1.5 kbar, respectively, for individual mineral-melt or mineral–mineral pairs. Calculated temperatures for clinopyroxenes in the pillow lavas (1095 ± 36 °C), are lower than those of clinopyroxenes in sheeted dikes type-I (1200 ± 21 °C), sheeted dikes type-II (1177 ± 25 °C), and discrete dikes (1166 ± 121 °C) (see Supplementary Table 2). Considering the compositions of the minerals may have been changed during later-stage, lower-temperature processes, the calculated temperatures may represent the minimum values.

The primitive mantle-normalized trace element profiles of clinopyroxene from the studied rocks exhibit generally substantial negative Ti and K anomalies (Fig. 9A–C). Large-ion lithophile elements (LILE), such as Sr and Ba are generally low, likely reflecting either early crystallization of plagioclase or melting of a depleted mantle source. Zr is depleted in Cpx of the pillow lava samples, but shows either enrichment or mixed behavior in Cpx from the sheeted and discrete dike samples. Conspicuous enrichment in Y generally characterizes Cpx of the sheeted dikes. Nb is notably depleted in the sheeted dikes compared to the pillow lavas (Fig. 9A–C).

The Cpx have moderate abundances of REE, and display flat REE patterns with slight LREE depletions in Cpx from pillow lavas and enrichments in Cpx from sheeted and discrete dikes (Fig. 9D–F). Cpx from the discrete dikes has characteristically elevated REE concentrations relative to the other sheeted dikes and pillow lavas (58–106 ppm versus 37–81 ppm, respectively). Chondrite-normalized REE patterns of Cpx from pillow lavas show similarities with the N-MORB patterns and the sheeted dikes patterns are markedly similar to the E-MORB. The REE patterns of Cpx from the discrete dike samples resemble OIB patterns. Compared to Cpx from other studied volcanic rocks, the diagnostic negative Eu anomalies in the discrete dikes (Fig. 9F) are consistent with crystallization of trapped melt fractions in equilibrium with plagioclase.

5. Petrogenetic modeling

5.1. Magma types and geotectonic environment implications

The volcanic rocks of the Wadi Ghadir ophiolite show geochemical features that correspond to mixed MORB-like and arc-related geochemical signatures. More specifically, the rocks are subalkaline basalts and basaltic andesites (Fig. 5A, B) with variable La/Sm_N (0.5–3.9), low MgO (2.0–7.2 wt%) and high Dy/Yb_N ratios (1.1–1.8). The pillow lava and both types of sheeted dikes have generally low Al_2O_3/TiO_2 and CaO/TiO_2 ratios (mostly ≪ 10), typical of high-Ti type basic volcanics (Sun and Nesbitt, 1978). By contrast, the discrete dikes are low-Ti basalts and basaltic andesites with distinctively higher Al_2O_3, CaO and MgO contents, and Al_2O_3/TiO_2 and CaO/TiO_2 ratios higher than chondritic values (20 and 17, respectively). The sheeted dikes and the pillow lava samples plot mainly in the transitional field and a few samples plot in the tholeiitic field (Fig. 5C). Only the discrete dikes and many of the Abd El-Rahman et al. (2009) samples plot in the calc-alkaline fields (Fig. 5C).

The pillow lavas and sheeted dikes samples have compositions above the MORB-OIB mantle array, and overlap the field of back-arc basalts (Fig. 6A). Compared to the sheeted dikes, the discrete dikes preserve geochemical affinities of calc-alkaline lavas and island–arc tholeiites. Each unit of the investigated volcanic rocks exhibits a distinct primitive mantle-normalized REE pattern (Fig. 7D–F). The striking features include pillow lavas with LREE = 1.5–3.3 × N-MORB, $(La/Yb)_N$ = 1.5–3.1; $(La/Yb)_N$ = 1.9–5.1; sheeted dike blocks in the mélange (type-I): LREE = 0.6–1.1 × N-MORB, $(La/Yb)_N$ = 0.8–1.0; and sheeted dikes cutting the gabbro complex (type-II) with LREE = 2.6–4.4 × N-MORB. Pillow lavas with E-MORB-like REE characteristics and the sheeted dikes (type-I) with REE patterns analogous to the N-MORB (Fig. 7D–F) may reflect increasing contamination of the mantle source by subduction components. The largely E-MORB-similar trace element compositions of the pillow lavas and dike complexes can be explained by 10% melting of contaminated source (with nearly 2–4% subduction-involved components). Fractional crystallization and simultaneous crustal assimilation rate was >0.6. The discrete dikes with LREE = 1.5–2.2 × N-MORB, $(La/Yb)_N$ = 4.8–6.6 probably represent the most fractionated LREE patterns and most likely manifest markedly different melts. Enrichments in Zr relative to the primitive mantle composition is more pronounced in the sheeted dikes type-I and discrete dikes, suggestive of contributions from crustal components relative to the pillow lavas and sheeted dikes type-II (e.g., Pearce and Peate, 1995).

The trace elements and REE patterns of clinopyroxenes from the different types of the investigated volcanic rocks imitate their whole-rock patterns (Fig. 9). Negative Ti anomalies characterize clinopyroxene from type-I and type-II sheeted dikes and the discrete dikes (Fig. 9A–C), suggesting subduction-related processes, but fractionation may have led to the absence of negative Ti in the whole-rock patterns of the host rocks (Fig. 7A–C). Clinopyroxenes from the pillow lavas have relatively restricted Y/Nb (11–20.7) and Zr/Nb (2.6–9.4) ratios compared to higher and highly variable values for the sheeted dikes and the discrete dikes (21.5–157.2 and 25.8–218.7; 8.8–317.9 and 22.5–90.5, respectively). Cpx grains from the sheeted dikes type-I have consistently lower Nb/Th ratios (0.4–5.3) compared to characteristically higher values for clinopyroxenes from the pillow lavas and the other dikes types (sheeted dikes type-II and discrete dikes). This feature suggests that the effect of slab-associated components/fluids was insignificant in the mantle source of the sheeted dikes type-I (e.g., Sun and McDonough 1989; Ionov and Hofmann 1995; Pearce and Peate 1995).

5.2. Primary melt composition and melting conditions

The variable amounts of clinopyroxene and plagioclase phenocrysts combined with the low Mg# values and Ni and Cr concentrations in the investigated ophiolitic volcanic rocks suggest that their melts were not equilibrated with mantle peridotites. Fractional crystallization could have substantially modified the primary composition of these melts. The Petrolog3 software (Danyushevsky and Plechov, 2011) is used to determine the composition of primitive magmas for the volcanic rocks prior to fractional crystallization. This software incorporates numerous mineral-melt equilibrium models to simulate crystallization and model reverse fractional crystallization at variable pressure, melt oxidation state and H_2O contents (Nielsen and Dungan, 1983). The initial oxidation state of magma is set to QMF + 1 (e.g., Pearce and Robinson, 2011). Slightly hydrous melting conditions were considered for the back-arc tholeiitic MORB-like magma (assigned for the Wadi Ghadir pillow lavas), by assuming water contents of 1 wt% (Zimmer et al., 2010), whereas higher water contents of 4 wt% were regarded as appropriate for the calc-alkaline melts produced the discrete dikes, as suggested by Plank et al., (2013). In either cases, reverse fractional crystallization

Table 1
Summary of the results of calculations of the primary magma compositions from Petrolog results for clinopyroxene and Cr-Spinel, and PRIMELT3 for olivine fractionation.

	Pillow lava		Dikes-type-I		Dikes-type-II		Discrete dikes	
	Ave.	1SE	Ave.	1SE	Ave.	1SE	ave.	1SE
SiO_2	51.10	0.45	52.69	0.74	50.51	0.67	51.14	0.19
TiO_2	2.79	0.43	1.04	0.12	1.35	0.42	0.49	0.07
Al_2O_3	12.11	1.05	13.94	0.55	12.66	0.81	15.00	0.45
FeO	5.94	0.14	6.15	0.10	6.75	0.12	6.33	0.04
Fe_2O_3	2.05	0.44	0.43	0.22	1.66	0.51	0.40	0.05
MnO	0.24	0.02	0.17	0.01	0.20	0.01	0.21	0.02
MgO	10.22	0.38	10.29	0.25	11.60	0.39	10.61	0.29
CaO	12.15	0.22	12.41	0.24	12.66	0.27	12.60	0.21
Na_2O	2.67	0.19	2.46	0.21	1.95	0.08	2.19	0.15
K_2O	0.24	0.06	0.21	0.02	0.35	0.02	0.70	0.09
P_2O_5	0.41	0.07	0.16	0.01	0.24	0.03	0.25	0.08
Cr_2O_3	0.03	0.00	0.05	0.03	0.04	0.01	0.05	0.01
NiO	0.06	0.01	0.04	0.01	0.02	0.00	0.03	0.00
Mg#	63.21	0.51	62.61	0.39	63.20	1.07	62.65	0.49
Mantle potential Temp. Tp (°C)	1274	8.21	1291	4.16	1324	5.97	1301	3.77
Partial Melt. Deg. (F%)	5.83	1.17	10.00	0.82	13.00	2.00	12.00	1.15
Pressure (kbars)	8.40	0.37	9.73	2.49	14.75	1.42	10.73	0.62
% Ol fractionated	10.97	1.44	9.43	1.49	6.93	1.87	8.50	1.12
% Cpx fractionated	40.33	3.27	37.25	3.20	37.50	2.89	37.00	5.72
% Cr-Sp fractionated	0.55	0.16	0.15	0.06	0.33	0.17	0.18	0.05

Mantle potential temperatures Tp and partial melting degrees *F* as determined by the PRIMELT3 software. Pressure calculations are based on Lee et al. (2009)'s geobarometer.

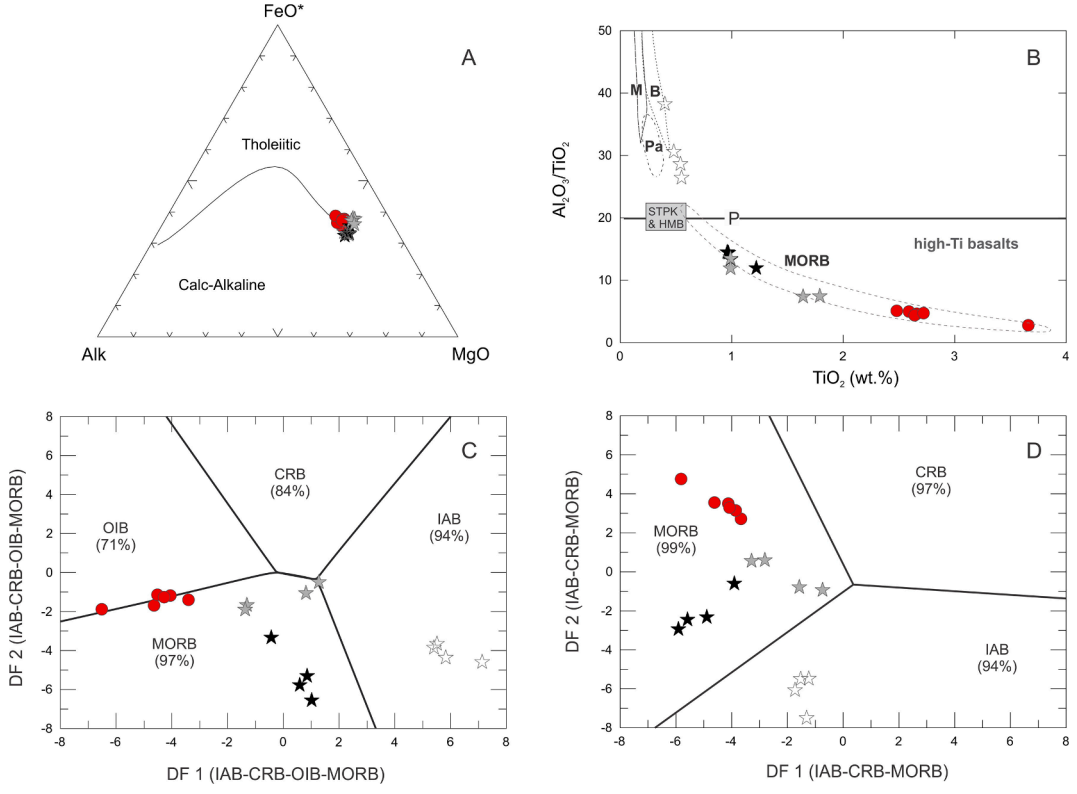

Fig. 10. (A) ($K_2O + Na_2O$)–FeO^T–MgO (AFM) diagram of Irvine and Baragar (1971) with the calculated primary melt compositions for the Wadi Ghadir ophiolitic volcanics, (B) TiO_2 vs. Al_2O_3/TiO_2 variation in different basalts (after Sun and Nesbitt, 1978). Fields of different basalts include Archaean spinifex– textured peridotitic komatiites (STPK), high-Mg basalts (HMB), MORB, island-arc basalts (Pa – Papua; M – Mariana Trench), and ophiolitic basalts (B – Betts Cove). "P" is model pyrolite, (C) Discrimination diagram IAB-CRB-OIB-MORB with data points for melts calculated for the Wadi Ghadir ophiolitic volcanics. The fields are: IAB = island arc basic rocks; CRB = continental rift basic rocks; OIB = Ocean island basic rocks; MORB = Mid-Ocean Ridge basic rocks. The percentages next to the field names refer to the percentage of the correct classification as inferred in the original paper by Agrawal et al. (2004), (D) Discrimination diagram for three of the four groups (IAB-CRB-OIB-MORB) of tectonic settings at a time (Agrawal et al., 2004).

calculations were done by assuming that clinopyroxene and Cr-spinel were the liquidus phases. Primary melt calculations were accomplished by considering polybaric crystallization with pressures increasing from 1 kbar continuously up to 13 kbar. Application of the Petrolog3 program reveals that clinopyroxene was indeed the main fractionating phase for the tholeiitic, as well as for the arc-related melts, whereas Cr-spinel was partially removed from the melts (Table 1, Supplementary Table 3). Clinopyroxene as the main fractionating phase is further confirmed from the petrographic observations that reveal the frequent presence of corroded clinopyroxene phenocrysts in the analyzed samples.

The parental magma compositions prior to olivine fractionation were estimated by the PRIMELT3 software (Herzberg and Asimow, 2015) and using the results of Petrolog3 for the primitive melts. The PRIMELT3 software is designed to determine the composition and temperature of primary magmas from primitive lavas by successive additions or subtractions of equilibrium olivine. Despite the fact that PRIMELT3 is calibrated by melting experiments on fertile and dry peridotites, uncertainties in fertile peridotite composition do not propagate significant errors in the resultant mantle T_P calculations (Herzberg and Asimow, 2015). Calculations were applied assuming accumulated fractional melting, whereas the $Fe^{2+}/\Sigma Fe$ ratio was set to 0.85 for the pillow lava magma series (tholeiitic MORB-like) and to 0.82 for the different dike complexes magma series. These values were selected based on the average oxidation conditions that are expected for magmas that are either slightly or significantly affected by slab-derived fluids, typical of back-arc systems (Kelley and Cottrell, 2009).

Mantle potential temperatures have been calculated by using the primary magma compositions (after Ol, Cpx and minor Pl fractionation; see Supplementary Table 3) in the PRIMELT3 software. Results show that the average mantle potential temperature for the pillow lavas melt was ~1275 °C, overlapping the range of MORB-related ambient mantle magmas (e.g., Putirka et al., 2007; Herzberg and Asimow, 2015). The calculated temperature range for the sheeted dikes type-I melt is ~1290 °C, and for the sheeted dikes type-II melt is ~1325 °C. The discrete dikes melt is estimated to have had mantle potential temperature of ~1300 °C. Variability deduced from the estimated partial melting degrees for each one of the melt series by the PRIMELT3 software also correspond to the different types of these rocks. Melt for the pillow lavas was formed by 6 ± 1% partial melting of the mantle source, whereas the sheeted dikes type-I melt was produced by 10 ± 1% partial melting. Melts of sheeted dikes type-II and discrete dikes were produced by higher degrees of partial melting (~13 ± 2% and ~12 ± 1%, respectively) of fertile mantle peridotite. The enhanced partial melting degrees are likely associated with increasing influence of slab-derived fluids in the supra-subduction realm. The elevated TiO_2 contents in the calculated pillow lavas melt may be attributed to a source characteristic, reflecting the mantle source fertility. By applying the geobarometer of Lee et al. (2009), pressure conditions during magma segregation for pillow lava melt (ave. 8.4 ± 0.4 kbar) yield moderate melting depths (30–35 km). Pressure estimates for the sheeted dikes type-I melt and sheeted dikes type-II melt are 9.7 ± 2.5 kbar and 14.7 ± 1.4 kbar, respectively. For the discrete dikes melt, estimated pressure conditions for the melt production are 10.7 ± 0.6 kbar. This pressure estimate may not reflect the depth of melts particularly when considering the recurrent switching from lithostatic to hydrostatic pressures assuming progressive wet melting for the sheeted dikes type-II and the discrete dikes melts.

The calculated primary melt compositions for the Wadi Ghadir ophiolitic volcanic rocks straddle the boundary between tholeiitic and calc-alkaline fields (Fig. 10A). In Fig. 10B, the calculated primary melts of the pillow lava and sheeted dikes type-I and type-II samples are classified as MORB, whereas the melt estimated for the discrete dikes plot in the low-Ti basalts on the brink of the ophiolitic and island arc basalts. According to Sun and Nesbitt (1978), high-Ti basalts have Al_2O_3/TiO_2, and CaO/TiO_2 ratios either similar to or less than chondritic

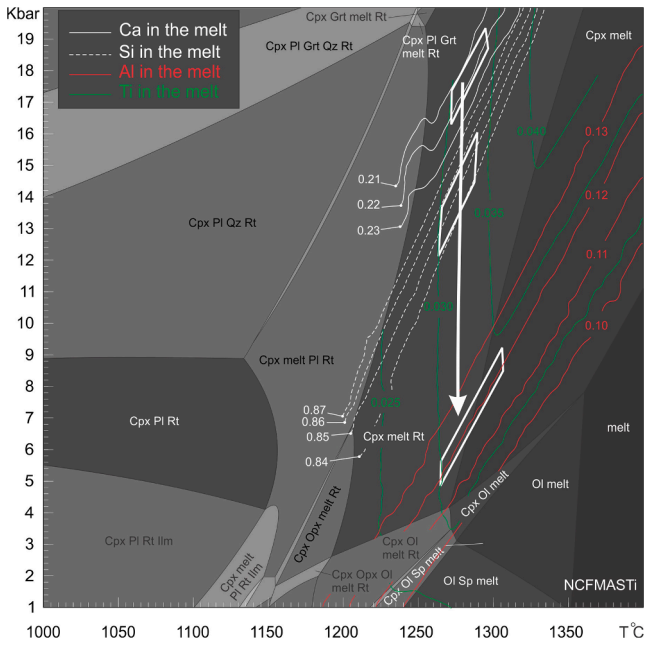

Fig. 11. P-T pseudosection of calculated primary magma with the following composition (SiO_2: 52.61; TiO_2: 2.39; Al_2O_3: 7.62; FeO: 8.48; CaO: 12.42; MgO: 12.22; Na_2O: 2.39 (mass amount)). The diagram model the formation of primitive magma for the Wadi Ghadir ophiolitic pillow lavas. The thermodynamic modeling was performed using the solution models and the thermodynamic data from Dale et al. (2000). The white arrow shows the isothermal decompression path suggested to produce the melt, whereas the intersections of different isopleths depict succeeding melting batches.

values (20 and 17 respectively). Basalts that are derived from MORB-type magma have high titanium (>0.7 wt% TiO_2) contents, whereas basalts from island-arc and inter-arc basins have low titanium (<0.4 wt % TiO_2) (Sun and Nesbitt, 1978). Fig. 10B shows that the calculated melts are generally MORB-type, highly comparable to the average estimated primary MORB as described by Gale et al. (2013). Increasing the degrees of melting of the mantle could produce higher Al_2O_3/TiO_2 in the melts (Sun and Nesbitt, 1977). The rocks are high-Ti type and show an increase in the degree of partial melting from the pillow lava to the discrete dikes (Fig. 10B).

In the discriminant diagrams proposed by Agrawal et al (2004) (Fig. 10C), melts calculated for the pillow lava and sheeted dikes plot mainly in the MORB field, whereas the melt for the discrete dikes plot in the IAB field. Melts for the pillow lavas transcend the MORB field to the OIB field. This assumption is further confirmed by Fig. 10D which shows dominant MORB for the pillow lava and sheeted dikes melts, while the discrete dikes are likely IAB.

6. Assessment of the melt evolution (thermodynamic modeling)

Conditions that controlled the magma generation processes during the formation of the Wadi Ghadir pillow lavas and the different dike complexes (i.e., pressure, temperature, and water contents) are modeled as thermodynamic *P-T* pseudosections in the NCFMASTi chemical system (i.e. Na_2O, CaO, FeO, MgO, Al_2O_3, SiO_2, TiO_2). The *P-T* pseudosections are *iso*-chemical phase equilibrium models showing the stable mineral phases at different P-T for a given bulk composition. Pseudosections presented here are calculated using Perple_X version 6.9.0 (Connolly and Kerrick, 1987; Connolly, 1990, 2005), and by employing the recent internally consistent dataset hp633ver of Holland and Powell (2011). The applied activity-composition models included: melt, garnet, olivine, orthopyroxene, clinopyroxene and spinel (Holland et al., 2018); plagioclase (Jennings and Holland, 2015); clino-amphibole (Dale et al.,

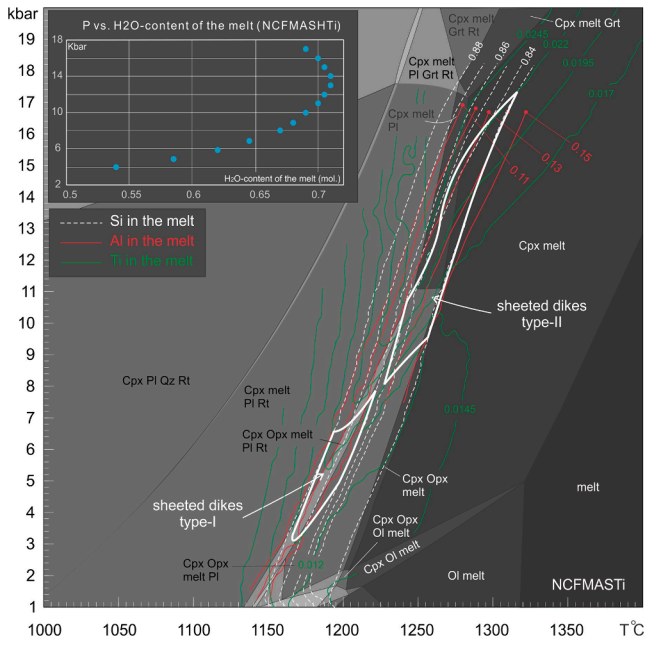

Fig. 12. P-T pseudosection of calculated primary magma with the following composition (SiO_2: 52.24; TiO_2: 1.81; Al_2O_3: 11.72; FeO: 7.98; CaO: 10.57; MgO: 11.48; Na_2O: 2.29 (mass amount)). The diagram models the formation of the sheeted dikes magma. Sheeted dikes type-II and type-I have different chemistry. Oxide isopleths indicate that the magma of the sheeted dikes type-II was formed at a higher pressure and temperature conditions than the magma of type-I. The insert shows the pressure vs·H_2O-content of the melt and shows a strong positive correlation (below 14 kbar) between the H_2O and the pressure which may indicate the potential role of the hydrostatic pressure. The pressure vs·H_2O-content of the melt was calculated in the NCFMASHTi using the same bulk as the P-T pseudosection and assuming the H_2O as an in-excess component to model in open-system conditions.

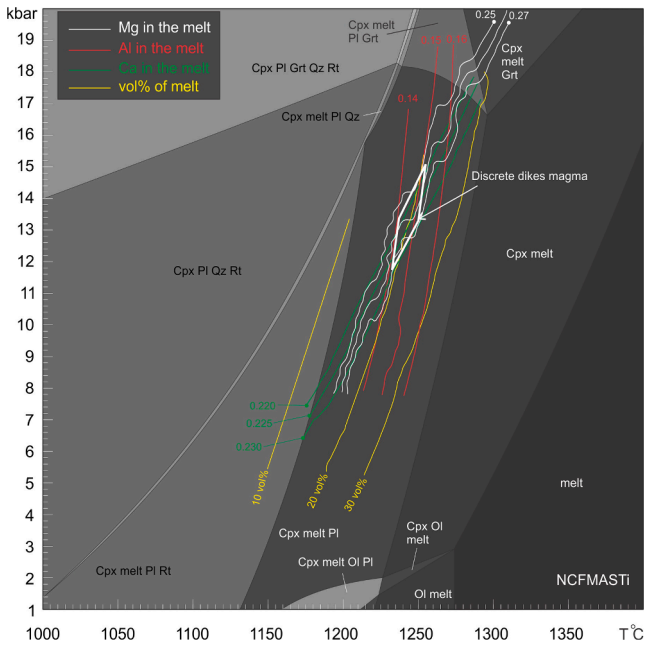

Fig. 13. A P-T pseudosection for the estimated calculated primary magma with the following composition (SiO_2: 54.60; TiO_2: 1.05; Al_2O_3: 14.29; FeO: 6.82; CaO: 8.20; MgO: 9.88; Na_2O: 3.20 (mass amount)). The white polygon represents the modeled condition under which the discrete dikes melts generated. Isopleths for melt proportion (vol%) have been plotted in the area of interest.

2000) and ideal solution model was used for *ortho*-amphibole. Mineral abbreviations presented here are after Whitney and Evans (2010).

6.1. *Mantle source of pillow lavas*

In order to model the development of the pillow lava magma, a pseudosection of the primary melt was calculated for a *P-T* range of 1–20 kbar and 1000–1400 °C (Fig. 11). The average composition calculated for the primary melt of the pillow lavas was used for the pseudosection calculations.

The pseudosection shows that the melt was a stable phase at conditions >1100 °C at 1 kbar. The lower-temperature limits of the melt-bearing fields increase with increasing the pressure (i.e., 1150 °C at 10 kbar). The clinopyroxene is stable at the entire *P-T* range of the pseudosection except for the higher temperature-low pressure conditions, particularly in the range of 1250 °C at 1 kbar – 1400 °C at 11 kbar). The orthopyroxene is stable below 6.5 kbar and under a narrow temperature range (1150–1200 °C). Olivine is stable at low-pressure conditions (i.e., <8 kbar) and under temperatures of 1150–1350 °C.

In order to constrain the origin and evolution of the pillow lava magma, melt composition (i.e., Ca, Si, Al and Ti isopleths) of the primary calculated magma (Supplementary Table 3) was employed in the pseudosection. The melt composition isopleths indicate that the melt was generated over a wide pressure range (19–5 kbar) but restricted temperatures, i.e., 1260–1300 °C (Fig. 11). The Ca and the Ti concentrations of the calculated primary magma indicate that the magma that generated the pillow lavas was initially generated at pressures of 19–16 kbar at an estimated temperature range (1270–1295 °C). The composition of the melt was buffered along with the Ti isopleths until lower pressure conditions attained. The Ti and Si isopleths of the primary magma intersect at 16–12.5 kbar and 1260–1290 °C. The Ti and Al isopleths indicate that the last stage of melt generation occurred at pressures ranging between 5 kbar and 9 kbar and temperatures between 1260 °C and 1300 °C.

Pressure conditions estimated to account for Ca and Si contents in the primitive magma are higher (i.e., 12.5–19 kbar) than the anticipated range of the reverse modeling calculations. However, the equilibrium conditions to accommodate the Ti and Al in the primitive magma (i.e., 9–5 kbar) are equivalent to the maximum pressure calculated by Cr-in-clinopyroxene barometer and the reverse modeling calculations (Supplementary Table 3). Moreover, the suggested temperature conditions from the pseudosection modeling are in good agreement with the mantle potential temperature designed by the reverse modeling.

Different melt composition isopleths indicate that the pillow lava magma was generated by isothermal decompression of a spinel lherzolite mantle at a wide pressure range (19–5 kbar) but a narrow temperature range of 1260–1300 °C (Fig. 11). Ti-bearing minerals played the main role in controlling and buffering the resultant melt composition, and the magma major element composition remained nearly unchanged under low pressure conditions (5–9 kbar).

6.2. *Mantle source of sheeted dikes*

The *P-T* pseudosection of the primitive magma for the sheeted dikes (Fig. 12), based on the results of petrological modeling (section 5), shows that the melt is a stable phase in the higher temperature part of the pseudosection. Melt-only- and melt + olivine-bearing fields are stable at high-temperature and low-pressure conditions (e.g., >1225 °C at 1.5 kbar and 1400 °C at <12.5 kbar). Clinopyroxene is a stable phase at low-temperature conditions (e.g., <1225 °C at 1.5 kbar; <1325 °C at 5 kbar). Orthopyroxene is stable at low-pressure conditions (i.e., <2.2 kbar) but under a restricted temperature range (1150–1212 °C). The rutile- and plagioclase-bearing assemblages are stable at the low-temperature part of the pseudosection, while the garnet-bearing assemblages are stable at the high-pressure (e.g., >13.2 kbar) part of the pseudosection.

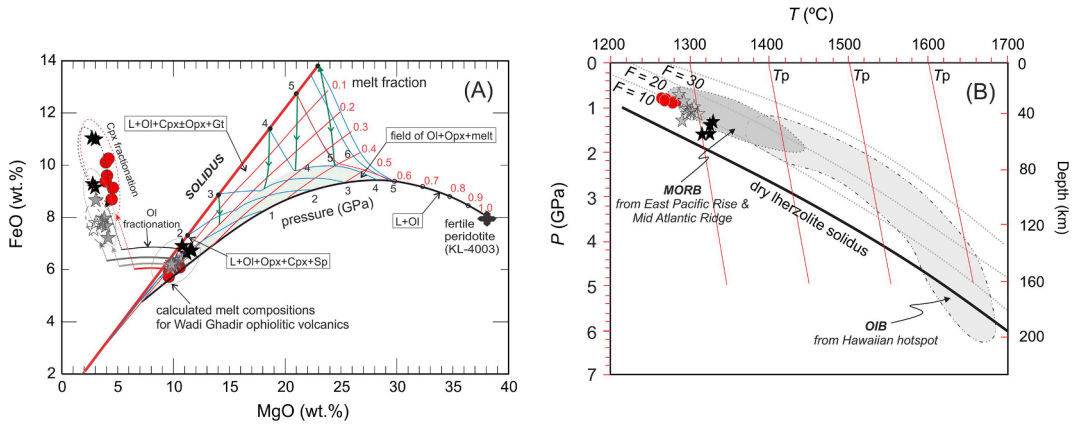

Fig. 14. (A) Primary magma calculation of peridotite melting in the binary MgO-FeO projection space integrated with an inverse model of olivine addition (adopted from Herzberg et al., 2007). The fractional partial melt compositions of fertile peridotite (KR-4003; from Herzberg and O'Hara, 2002) are estimated using reverse crystallization models. The thick red line represents liquid compositions on the solidus; thin red lines depict melt fractions with respect to initial fertile mantle source; green line represents accumulated fractional melt compositions that form during initial decompression melting whereas blue lines depict final melting pressure conditions, (B) Melting temperatures and pressures calculated for the Wadi Ghadir ophiolitic volcanics. Lherzolite solidus and melt fraction isopleths are from Katz et al. (2003). Curved lines represent melting adiabats, red lines represent solid mantle adiabats (modified from Lee et al., 2009). Hawaiian hotspot source regions for shield and post-shield basalts are modified from Lee et al. (2009). Temperatures and pressures ranges for MORB from the East Pacific Rise and Mid-Atlantic Ridge are from Lee et al. (2009).

Isopleths for the primitive melt composition of the sheeted dikes (Mg, Ca, Si, Al and Ti) are consistently parallel. For simplification, only the Si, Al and Ti isopleths are shown in the pseudosection (Fig. 12). The sheeted dikes type-I and type-II show distinct compositional ranges. The Ti content (i.e., 0.12–0.15 mol.%) of the type-I sheeted dikes intersects the Al and the Si isopleths and indicates magma generation at 7.8–3 kbar and 1170–1220 °C. Although the lower pressure limit (3 kbar) of the estimated condition is lower than the pressure calculated by the reverse modeling, the upper-pressure limits are in agreement (~7.8–7 kbar). The chemistry of type-II sheeted dikes indicates higher pressure and temperature conditions than type-I. The Ti isopleths intersect the isopleths of Si and Al in a wide range of pressure (17–8.5 kbar) but in a relatively restricted temperature range of 1230–1310 °C (Fig. 12). Both the estimated pressure and the temperature conditions are in agreement with the results of the reverse modeling.

The similarly between magma generation conditions of the type-I and the type-II sheeted dikes may indicate a common origin. The sheeted dikes magma was produced under temperatures of 1170–1310 °C and at pressures ranging from 17 to 3 kbar. The higher pressure estimate may reflect hydrostatic instead of lithostatic pressure. The H_2O content in the produced magma was modeled in the NCFMASHTi chemical system. The relationship between the pressure and the H_2O content (the inset in Fig. 12) indicates a strong positive correlation. This relationship suggests that the magmas of both type-I and type-II sheeted dikes were formed at similar lithospheric depths, but likely under varied water contents, demonstrated by varied hydrostatic pressure conditions.

6.3. *Mantle source of discrete dikes*

The clinopyroxene is the only stable pyroxene phase that is observed in the pseudosection of the discrete dikes (Fig. 13). The clinopyroxene is a stable phase in all the fields of the calculated pseudosection, except the melt-only and the melt + olivine assemblages. Plagioclase and rutile are stable minerals at the low-temperature assemblages of the pseudosection, whereas garnet is a stable phase in the high-pressure assemblages.

Mg, Al and Ca isopleths of the primitive melt composition (Supplementary Table 3) intersect at 15–12 kbar and 1230–1260 °C. The estimated mantle potential temperature from the pseudosection modeling is slightly lower than the temperature calculated by reverse modeling (i.e., 1296–1305 °C), but both estimations are in the error range of the methods used. The pressure estimated from the pseudosection modeling is 1–2 kbar higher than that calculated by reverse modeling (i.e., 11.4–9.9 kbar). The volume of the primitive melt produced at these conditions is around 15–30% of the total volume of the system (Fig. 13). Pseudosection modeling indicates that the magma for the discrete dikes was generated at restricted pressure and temperature conditions, suggesting an equilibrium between the melts and mantle peridotites at this stage.

7. Discussion

Formation of sheeted dike complexes in ophiolitic sections requires that the spreading rate and magma supply over several Myr is balanced (Robinson et al., 2008). This criterion is unlikely to be attained in supra-subduction zone environments. The occurrence of the sheeted complex in the Wadi Ghadir ophiolite suggests a MORB or back-arc setting. Considering the occurrence of a large infracrustal gneissic block (Wadi Hafafit culmination; Makroum, 2017 and references therein) to the west of the Wadi Ghadir ophiolite, the basin in which these ophiolitic rocks were formed is thought to have been a marginal oceanic basin. The pillow lavas with chemical characteristics of tholeiitic N-MORB, and sheeted dikes with transitional 'picritic' basalt geochemistry (E-MORB) may be attributed to variable degrees of partial melting of a spinel lherzolite mantle source (as manifested by consistent Dy/Yb < 3 in all of the studied rock; Jung et al., 2006) beneath a nascent arc–back-arc spreading center. The range of magma compositions in the investigated volcanic rocks and occurrences of fractionated plagiogranite in the gabbro complex (Kröner et al., 1992) are consistent with slow spreading rates which gave rise to polybaric, closed-system fractionation of magmas and periodic chamber abandonment. On the other hand, late discrete dikes with SiO_2 levels in the andesite range have low-TiO_2 contents and high Mg# may be analogous to fractionated equivalents of OIB or IAB. The observed positive variation of CaO with respect to MgO suggests accumulation of Ca-plagioclase phenocrysts during the crystallization of these discrete dikes. Development of the CA trend in back-arc basin melts is chiefly governed by magmatic waters as demonstrated by pMelts calculations and laboratory experiments (Zimmer et al., 2010). Such petrogenetic evolution of the oceanic crust may reflect subduction initiation by far-field geodynamic processes in an oceanic setting (Stern and de Wit, 2003; van Hinsbergen et al., 2015).

Compositional variations in magma series calculated for the Wadi

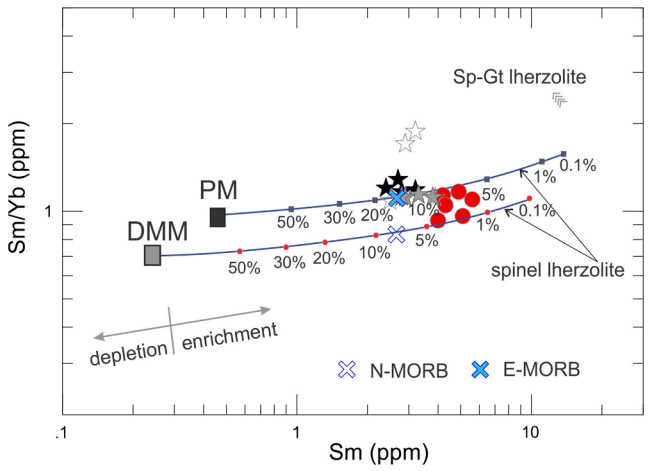

Fig. 15. Binary plot of Sm/Yb vs. Sm (calculated values in primary melts) displaying mantle sources and partial melting curves by applying the non-modal batch melting equation of Shaw (2000). Melting curves were drawn for spinel lherzolite, with mineral proportions of Ol 53.0% + Opx 20.0% + Cpx 17.0% + Sp 3.0% and melt mode proportions of Ol 6.0% + Opx 28.0% + Cpx 67.0% + Sp11% (Kinzler 1997). Partition coefficients are from McKenzie and O'nions (1991, 1995). Primitive Mantle (PM) and Depleted MORB Mantle (DMM) sources are from Sun and McDonough (1989) and Workman and Hart (2005), respectively. The given percentages correspond to primitive magmas calculated assuming Cpx fractionation only; Cpx addition for each magma series according to calculated values and taking into account the Sm and Yb contents from the corresponding LA-ICP-MS Cpx measurements. Red fit dots on the two lines depict partial melting degrees for the relevant mantle sources. Reverse Cpx fractionation was performed using the Rayleigh fractionation-based FC-modeler software (Keskin, 2002).

Ghadir ophiolitic volcanics may reflect different mantle source regions, various forms of melt-rock interaction and/or melt fractionation processes (e.g., Lambart et al., 2012; Brunelli et al., 2014). The similar Mg# suggests a common mantle source region, and suggests contamination and fractionation processes may account for the varied melt compositions of the studied rocks. The pillow lavas have geochemical features typical of the back-arc basin basalts (BABBs), which are generated by decompression melting similar to that of N-MORB, albeit with a mild hydrous and incompatible element enrichment coupled with a subduction component (elevated Th/Nb) (e.g., Gribble et al., 1996; Smith et al., 2001; Langmuir et al., 2006). The P-T pseudosection (Fig. 11) suggests an isothermal (i.e., 1260–1300 °C) decompression (from 19 to 5 kbar) path as a mechanism to generate the pillow lava magma. The sheeted dikes and discrete dikes magmas, with moderate enrichments (relative to MORB) in alkalis and other large ion lithophile elements, variable depletions in Ti, Nb and Y, and essentially flat rare earth element (REE) patterns, were likely produced by rigorous wet melting of the same spinel lherzolitic mantle source.

OIB- and E-MORB-type basaltic magmas in the intra-oceanic back-arc setting can be generated from plume-contaminated source regions, where the enriched plume material is brought into the depleted mantle wedge by the mantle flow around the slab via slab retreat (e.g., Fretzdorff et al., 2002; Gamal El Dien et al., 2021). Alternatively, E-MORB- and OIB-type basalts with no plume involvement have been attributed to decompression melting of enriched mantle source(s) in response to slab roll-back and retreating (e.g., Hickey-Vargas et al., 2006).

Temperatures of mantle partial melting that are derived from the primitive melt calculations are used to estimate the *T*p for each type of the investigated volcanic rocks (e.g., Putirka et al., 2003; Putirka, 2008; Lee et al., 2009; Herzberg and Asimow, 2015). The results indicate that the calculated *T*p values of Wadi Ghadir volcanics, by using the SiO_2-based thermobarometer, overlap with the global MORB array, but contrast with the *T*ps of the Hawaiian OIB array (Fig. 14). The MORB *T*p array represents the background upper-mantle temperature, whereas the *T*ps of the Iceland and Hawaii samples represent plume-affected mantle. The calculated *T*ps for the ophiolitic volcanics are similar to normal MORB, emphasizing the back-arc setting and discarding significant thermal anomaly in the upper mantle when they formed.

Pseudosection modeling indicates that the different types of magmas were generated within the stability field of clinopyroxene. Moreover, the melt compositions (calculated by the reverse modeling) show that the main fractionated phase in all melt types was clinopyroxene (37–40%). Sm, Yb and other heavy rare earth elements are preferably partitioned in clinopyroxene rather than in other silicate phases in spinel lherzolite (Green and Pearson, 1985). Data of the primitive magma compositions are plotted in the binary Sm vs. Sm/Yb space (Fig. 15) with two mantle sources; a fertile primitive mantle source (PM) and a depleted mantle source (DMM). The Sm vs. Sm/Yb plot examines whether mantle depletion may have contributed to magma diversity or whether changes of partial melting degrees and depth of melting were the main processes. These results agree with those deduced from the major oxide composition of the modeled melts (Supplementary Table 3). However, Fig. 15 shows that the pillow lavas may likely have been formed from a slightly more depleted mantle source, which would require lesser degrees of partial melting. On the other hand, melts for the sheeted dikes tend to display fairly elevated Sm/Yb ratios suggesting that they may have been derived from a slightly enriched mantle source. In either case, it is evident that mantle sources, despite restricted modifications, remained relatively fertile without experiencing any significant depletion, though source rocks were to some extent affected by subduction. An intrinsic spatial relationship between lava composition and depth to the subducted slab appears to be less direct in the back-arc basin compared to the island arc setting (Johnson and Sinton, 1990; Price et al., 1990; Plank and Langmuir, 1992; Sinton et al., 2003; Langmuir et al., 2006).

8. Conclusions

The geochemical characteristics of the Wadi Ghadir ophiolitic volcanic rocks and petrogenetic modeling of the primary melts support the evolution from an early-stage MORB-type activity that resulted in the restricted depletion of mantle peridotites, as well as the establishment of conditions that favored the circulation of slab-related fluids, which subsequently led to the formation of lavas with higher Mg contents. The MORB-like magmas could have resulted from partial melting as the initial magmatic expression during subduction initiation, followed by IAT 'SSZ-typical' lavas with partial melting of depleted peridotitic residue metasomatized by fluids derived from subducting oceanic crust and sediments. This scenario does not exclude that back-arc extension and slab-rollback produced MORB-like lavas in a SSZ realm (see Whattam and Stern, 2011), leading to backarc crustal and upper mantle units with different geochemical fingerprints (e.g., Furnes and Safonova, 2019).

Involvement of the subduction-related fluids/melts likely played a key role in triggering greater degrees of partial melting by lowering the peridotite solidus, which explains the apparently high potential mantle temperatures for dike complexes. The petrogenetic indicators retained by these dikes may be attributed to changes in depth of melting, or to the extent of partial melting, likely also associated with increasing influence of slab-derived fluids in an SSZ setting. The relatively late subduction initiation event, which led to the formation of the discrete dikes, can be explained by the induced model, where externally applied compressive stress and convergence simulated a convective instability can grow and self-sustaining subduction occurs (e.g., McKenzie, 1977; Toth and Gurnis, 1998).

Melt calculations based on the bulk-rock geochemistry and the LA-ICP-MS data of Cpx relicts allowed the recognition of four main magma series with tholeiitic basaltic andesite affected by restricted subduction-related fluids/processes, whereas the later type comprises OIB-like or IAT-like basalts with elevated Mg# and exhibits a calc-alkaline geochemical trend. Petrogenetic calculations and modeling

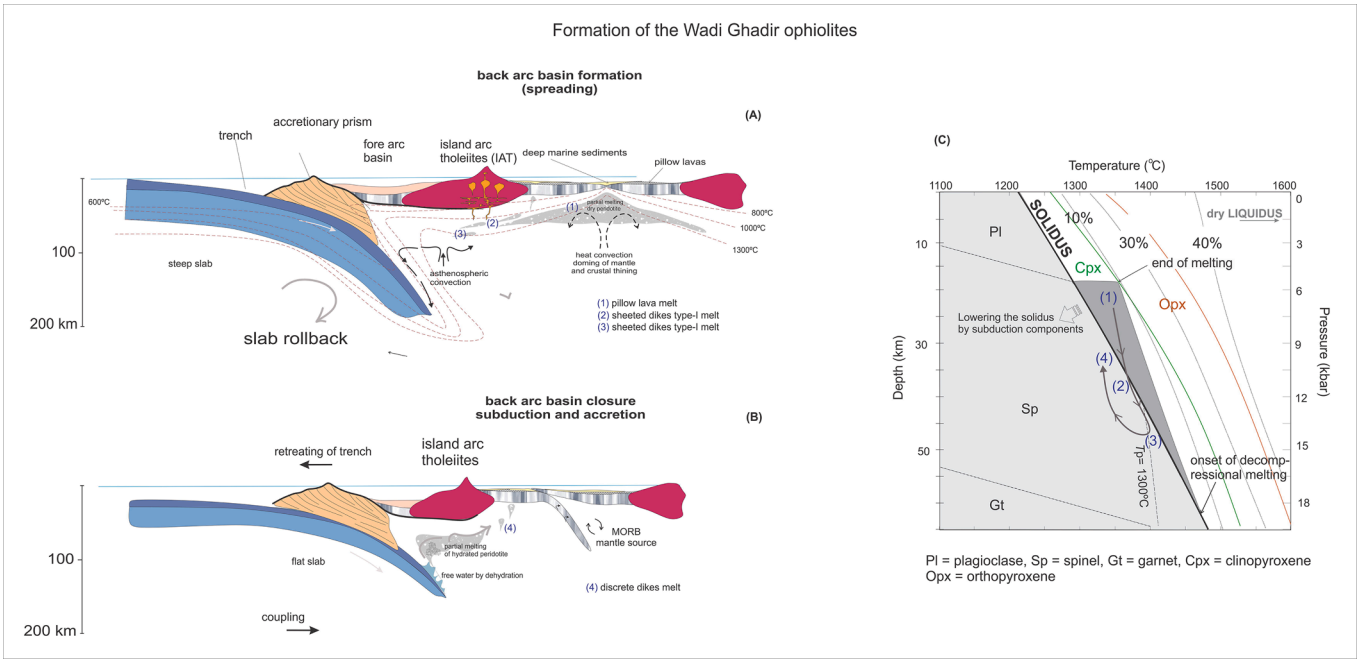

Fig. 16. Conceptual model of the petrogenesis of Wadi Ghadir back-arc ophiolites. (A) Schematic illustration of the oceanic mantle-crust section during the opening stage of the back-arc basin showing the inferred regions of mantle partial melting and the inferred locations of the N-MORB pillow lava and E-MORB sheeted dikes magmas, (B) The basin closure stage, subduction initiation and production of IAT magma (discrete dikes) from subduction-metasomatized mantle material, (C) P-T space shows the anticipated path of magma generation and evolution of the volcanic rocks of the Wadi Ghadir ophiolite. The experimentally determined dry solidus, melting percentage and stability regions for garnet, clinopyroxene and orthopyroxene are from Herzberg and O'Hara (2002). The sub-solidus stability fields of plagioclase, spinel and garnet are from McKenzie and O'nions (1991). The numbers on the P-T path are referred to the different types of magmas as in A and B. The P-T position of the pillow lava (i.e., #1) depicts the conditions for magma batch separation. All the magma types produced from spinel lherzolitic mantle source. Magma #3 and #4; the Type-II sheeted dikes and discrete dikes, respectively, were formed by lowering the solidus due association of external components/fluids.

show that these rocks experienced variable differentiation processes. The pillow lavás primary magma was formed under moderate partial melting conditions (~6 ± 1%) from MORB-like mantle. The magma was generated by an isothermal decompression path started at a depth equivalent to pressure 19 kbar and *T*p ≈ 1275 °C. Ti-bearing minerals controlled the melt composition to a constant depth equivalent to a pressure of 5 kbar, where the latest magma was extracted. The sheeted dikes type-I magma was formed under higher partial melting degrees (~10 ± 1%) and elevated *P-T* conditions (*T*p ≈ 1290 °C; P ≈ 9.7 ± 2.5 kbar). Although the magma of the sheeted dikes type-II was generated at *T*p ≈ 1325 °C and *P* ≈ 14.7 ± 1.4 kbar. The high-pressure conditions of the latter (comparing to the sheeted dikes type-I) suggests fluid infiltration from the subducting slab, leading to the enhanced hydrostatic pressure. Primary magma of the discrete dikes was generated at *T*p of 1230–1300 °C and pressure of ~10.7 ± 0.6 kbar, reflecting melting of a heterogeneously metasomatized spinel lherzolitic mantle source.

A schematic model suggested here for the evolution of the Wadi Ghadir ophiolite is given in Fig. 16. We assume that back-arc basin opening in a subduction setting occurred as a result of intrinsic slab rollback and trench retreat due to back-arc lithosphere extension and thinning (Fig. 16A). Far-field compressional regime, most likely linked with the E- and W-Gondwana assembly history (Collins et al., 2021) led to subduction initiation. This assumption is in agreement with the absence of a complete subduction girdle (a mantle downwelling zone) around Gondwana as suggested by Cawood et al. (2021).

During the slab rollback stage, partial melting of hitherto subduction-meatsomatized mantle regions could have produced the discrete dikes magma by flux melting of hot, attenuated back-arc mantle fluids/melts (Fig. 16B). Lowering the mantle peridotite solidus due the interaction with subduction fluids triggered melting below the anhydrous solidus (Fig. 16C). This scenario is consistent with the evolution from N-MORB to IAT magmas, with progressive maturing of the SSZ system. Melt formation and evolution in the Wadi Ghadir ophiolite may exemplify widespread mantle heterogeneity during the accretionary stages of the Arabian-Nubian Shield.

CRediT authorship contribution statement

Basem Zoheir: Conceptualization, Investigation, Writing – original draft, Writing – review & editing. **Aliaa Diab:** Conceptualization, Investigation. **Petros Koutsovitis:** Writing – original draft, Writing – review & editing. **Tamer Abu Alam:** Writing – original draft, Writing – review & editing. **Mark Feigenson:** Investigation. **Mohammed El-Bialy:** Writing – original draft. **Amr Abdelnasser:** Investigation.

Declaration of Competing Interest

The authors declare that they have no known competing financial interests or personal relationships that could have appeared to influence the work reported in this paper.

Acknowledgements

Basem Zoheir likes to acknowledge the Alexander von Humboldt foundation for supporting his research stay at Kiel University, making this research possible. Fuat Yavuz is thanked for the generous help he offered in the pyroxene thermobarometry calculations by using the WinPyrox program. B. Murphy, A. Ahmed and S. Arai are thanked for their constructive suggestions and comments, which helped to improve an earlier version of this paper.

Appendix A. Supplementary material

Supplementary data to this article can be found online at https://doi.org/10.1016/j.precamres.2021.106480.

References

Abd El-Naby, H., Frisch, W., Siebel, W., 2008. Tectono-metamorphic evolution of the Wadi Hafafit Culmination (central Eastern Desert, Egypt). Implication for Neoproterozoic core complex exhumation in NE Africa. Geologica Acta 16, 293–312.

Abd El-Rahman, Y.A., Polat, A., Dilek, Y., Fryer, B., El-Sharkawy, M., Sakran, S., 2009a. Geochemistry and tectonic evolution of the Neoproterozoic Wadi Ghadir ophiolite, Eastern Desert, Egypt. Lithos 113 (1-2), 158–178.

Abd El-Rahman, Y., Polat, A., Dilek, Y., Fryer, B.J., El-Sharkawy, M., Sakran, S., 2009b. Geochemistry and tectonic evolution of the Neoproterozoic incipient arcfore- arc crust in the Fawakhir area, Central Eastern Desert of Egypt. Precam. Res. 175 (1-4), 116–134.

Abd El-Rahman, Y., Polat, A., Dilek, Y., Kusky, M.T., El-Sharkawi, M., Said, A., 2012. Cryogenian ophiolite tectonics and metallogenic of the Central Eastern Desert of Egypt: Int. Geol. Rev. 54, 1870–1884.

Abd El-Wahed, M., Kamh, S., Ashmawy, M., Shebl, A., 2019. Transpressive Structures in the Ghadir Shear Belt, Eastern Desert, Egypt: Evidence for Partitioning of Oblique Convergence in the Arabian-Nubian Shield during Gondwana Agglutination. Acta Geol. Sin. 93 (6), 1614–1646.

Abdel-Karim, A.M., Ali, S., Helmy, H.M., El-Shafei, S.A., 2016. The Fore-arc setting of the Gerf ophiolite, Eastern Desert, Egypt: evidence from mineral chemistry and geochemistry of ultramafites. Lithos 263, 52–65.

Abdel-Karim, A.M., Soliman, M.M., El-Kazzaz, Y.A., Mazhar, A.A., Abdel-Gawad, G.M., 2001. Geological and Geochemical Characteristics of the Mafic-Ultramafic Rocks of Gabal Gerf Area, Southeastern Desert of Egypt. Ann. Geol. Surv. Egypt 24, 193–218.

Abdelsalam, M.G., Abdeen, M.M., Dowaidar, H.M., Stern, R.J., Abdelghaffar, A.A., 2003. Structural evolution of the Neoproterozoic Western Allaqi-Heiani suture, southeastern Egypt. Precam. Res. 124 (1), 87–104.

Agrawal, S., Guevara, M., Verma, S.P., 2004. Discriminant analysis applied to establish major-element field boundaries for tectonic varieties of basic rocks. Int. Geol. Rev. 46 (7), 575–594.

Ahmed, A.H., 2007. Diversity of platinum-group minerals in podiform chromitites of the late Proterozoic ophiolite, Eastern Desert, Egypt: genetic implications. Ore Geol. Rev. 32 (1-2), 1–19.

Ahmed, A.H., 2013. Highly depleted harzburgite–dunite–chromitite complexes from the Neoproterozoic ophiolite, south Eastern Desert, Egypt: A possible recycled upper mantle lithosphere. Precambr. Res. 233, 173–192.

Ahmed, A.H., Hanghøj, K., Kelemen, P.B., Hart, S.R., Arai, S., 2006. Osmium isotope systematics of the Proterozoic and Phanerozoic ophiolitic chromitites: in-situ ion probe analysis of primary Os-rich PGM. Earth Planet. Sci. Lett. 245 (3-4), 777–791.

Albarède, F., 2003. Geochemistry: An Introduction. Cambridge University Press, Cambridge, p. 355.

Ali, K.A., Azer, M.K., Gahlan, H.A., Wilde, S.A., Samuel, M.D., Stern, R.J., 2010. Age of formation and emplacement of Neoproterozoic ophiolites and related rocks along the Allaqi Suture, south Eastern Desert, Egypt. Gondwana Res. 18, 583–595.

Azer, M.K., Stern, R.J., 2007. Neoproterozoic (835–720 Ma) serpentinites in the Eastern Desert, Egypt: Fragments of the fore-arc mantle. J. Geol. 115, 457–472.

Basta, F.F., Maurice, A.E., Bakhit, B.R., Ali, K.A., Manton, W.I., 2011. Neoproterozoic contaminated MORB of Wadi Ghadir ophiolite, NE Africa: geochemical and Nd and Sr isotopic constraints. J. Afr. Earth Sci. 59 (2-3), 227–242.

Beccaluva, L., Serri, G., 1988. Boninitic and low-Ti subduction-related lavas from intraoceanic arc-backarc systems and low-Ti ophiolites: a reappraisal of their petrogenesis and original tectonic setting. Tectonophysics 146 (1-4), 291–315.

Bortolotti, V., Marroni, M., Pandolfi, L., Principi, G., Saccani, E., 2002. Interaction between mid-ocean ridge and subduction magmatism in Albanian ophiolites. J. Geol. 110 (5), 561–576.

Brunelli, D., Paganelli, E., Seyler, M., 2014. Percolation of enriched melts during incremental open-system melting in the spinel field: a REE approach to abyssal peridotites from the southwest Indian Ridge. Geochim. Cosmochim. Acta 127, 190–203.

Cawood, P.A., Martin, E.L., Murphy, J.B., Pisarevsky, S.A., 2021. Gondwana's interlinked peripheral orogens. Earth Planet. Sci. Lett. 568, 2021. https://doi.org/10.1016/j.epsl.2021.117057.

Collins, A.S., Blades, M.L., Merdith, A.S., Foden, J.D., 2021. Closure of the Proterozoic Mozambique Ocean was instigated by a late Tonian plate reorganization event. Commun. Earth Environ. 2, 75. https://doi.org/10.1038/s43247- 021-00149-z.

Connolly, J.A.D., 1990. Multivariable phase-diagrams - an algorithm based on generalized thermodynamics. Am. J. Sci. 290 (6), 666–718.

Connolly, J.A.D., 2005. Computation of phase equilibria by linear programming: A tool for geodynamic modeling and its application to subduction zone decarbonation. Earth Planet. Sci. Lett. 236 (1-2), 524–541.

Connolly, J.A.D., Kerrick, D.M., 1987. An algorithm and computer program for calculating composition phase diagrams. Calphad 11 (1), 1–55.

Conoco Coral, 1987. Stratigraphic Lexicon and Explanatory Notes to the Geological Map of Egypt, 1:500,000. Printed in Germany by Institute für Angewandte Geodasie, Berlin, p. 264p.

Cookenboo, H.O., Grütter, H.S., 2010. Mantle-derived indicator mineral compositions as applied to diamond exploration. Geochem.: Explor. Environ. Anal. 10 (1), 81–95.

Dale, J., Holland, T., Powell, R., 2000. Hornblende-garnet-plagioclase thermobarometry: a natural assemblage calibration of the thermodynamics of hornblende. Contrib. Mineral. Petrol. 140 (3), 353–362.

Danyushevsky, L.V., Plechov, P., 2011. Petrolog 3: Integrated software for modeling crystallization processes. Geochem. Geophys. Geosyst. 12 (7) n/a–n/a.

De Paolo, J., 1981. Trace element and isotopic effect of combined wallrock assimilation and fractional crystallization. Annu Rev. Earth Planet Sci. 53, 189–202.

Dietrich, H., Petrakakis, K., 1986. A linear algebraic method for the calculation of pyroxene endmember componentsDie Berechnung von Pyroxen-Endgliedern mit Methoden der Linearen Algebra. Tschermaks Mineralogische und Petrographische Mitteilungen 35 (4), 275–282.

Dilek, Y., Furnes, H., Shallo, M., 2008. Geochemistry of the Jurassic Mirdita Ophiolite (Albania) and the MORB to SSZ evolution of a marginal basin oceanic crust. Lithos 100 (1-4), 174–209.

Egyptian Geological Survey and Mineral Authority (EGSMA), 1997. Report on Geological, Drilling and Geophysical Studies (Pumping Stations Site and Outlet of South Valley Canal), Tushka Area, 163p.

El Gaby, S., 1983. Architecture of the Egyptian basement complex. Proceedings of the Fifth International conference Basement tectonics, Cairo, Abstract, 19–20.

El-Bayoumi, R.M., 1980. Ophiolites and associated rocks of Wadi Ghadir, east of Gabal Zabara, Eastern Desert, Egypt. Ph.D. Thesis, Cairo University, Egypt, 171.

El-Bayoumi, R.M., 1983. Ophiolites and mélange complex of Wadi Ghadir Area, Eastern Desert, Egypt. Bull. Fac. Earth Sci King Abdulaziz University 6, 329–342.

El-Sayed, M.M., Furnes, H., Mohamed, F.H., 1999. Geochemical constraints on the tectonomagmatic evolution of the late Precambrian Fawakhir ophiolite, Central Eastern Desert, Egypt. J. Afr. Earth Sci. 29, 515–533.

El-Sharkawy, M.A., El Bayoumi, R.M., 1979. The ophiolites of Wadi Ghadir area, Eastern Desert, Egypt. Ann. Geol. Surv. Egypt 9, 125–135.

Farahat, E.S., El Mahalawi, M.M., Hoinkes, G., 2004. Continental back-arc basin origin of some ophiolites from the Eastern Desert of Egypt. Mineral. Petrol. 82, 81–104.

Fretzdorff, S., Livermore, R.A., Devey, C.W., Leat, P.T., Stoffers, P., 2002. Petrogenesis of the back-arc East Scotia Ridge, South Atlantic Ocean. J. Petrol. 43, 1435–1467.

Fritz, H., Abdelsalam, M., Ali, K.A., Bingen, B., Collins, A., Fowler, A.R., Ghebrab, W., Hauzenberger, C.A., Johnson, P., Kusky, T., Macey, P., Muhongo, S., Stern, R.J., Viola, G., 2013. Orogen styles in the East African Orogens: A review of Neoproterozoic to early Phanerozoic tectonic evolution. J. Afr. Earth. Sci. 86, 65–106.

Furnes, H., Safonova, I., 2019. Ophiolites of the Central Asian Orogenic Belt: Geochemical and petrological characterization and tectonic settings. Geosci. Front. 10 (4), 1255–1284.

Furnes, H., Thorseth, I.H., Tumyr, O., Torsvik, T., Fisk, M.R., 1996. Microbial activity in the alteration of glass from pillow lavas from Hole 896A, in Proceedings of the Ocean Drilling Program, Scientific Results 148, 191–206.

Gamal El Dien, H., Hamdy, M., Abu El-Ela, A., Abu-Alam, T., Hassan, A., Kil, Y., Mizukami, T., Soda, Y., 2016. Neoproterozoic serpentinites from the Eastern Desert of Egypt: Insights into Neoproterozoic mantle geodynamics and processes beneath the Arabian-Nubian Shield. Precam. Res. 286, 213–233.

Gamal El Dien, H., Li, Z., Abu Anbar, M., Doucet, L.S., Murphy, J.B., Evans, N.J., Xia, X., Li, J., 2021. Two-stage crustal growth in the Arabian-Nubian shield: initial arc accretion followed by plume-induced crustal reworking. Precambrian Res. 359, 106211.

Golich, A.N., Vysotskiy, S.V., 2020. Island-Arc Ophiolites of the Hahajima Seamount (Bonin Trench, Philippine Sea). Russ. J. Pacific Geol. 14, 221–240.

Green, T.H., Pearson, N.J., 1985. Experimental determination of REE partition coefficients between amphibole and basaltic to andesitic liquids at high pressure. Geochim. Cosmochim. Acta 49, 465–468.

Gribble, R.F., Stern, R.J., Bloomer, S.H., Stüben, D., O'Hearn, T., Newman, S., 1996. MORB mantle and subduction components interact to generate basalts in the southern Mariana Trough back-arc basin. Geochim. Cosmochim. Acta 60, 2153–2166.

Griffin, W.L., Powell, W.J., Pearson, N.J., O'Reilly, S.Y., 2008. GLITTER: data reduction software for laser ablation ICP-MS. In: Sylvester P (Ed.), Laser Ablation–ICP–MS in the earth sciences. Mineral Assoc Canada Short Course Series vol 40, Appendix 2, pp. 204–207.

Herzberg, C., Asimow, P.D., 2015. PRIMELT3 MEGA.XLSM software for primary magma calculation: Peridotite primary magma MgO contents from the liquidus to the solidus. Geochem. Geophys. Geosyst. 16, 563–578.

Herzberg, C., Asimow, P.D., Arndt, N., Niu, Y., Lesher, C.M., Fitton, J.G., Cheadle, M.J., Saunders, A.D., 2007. Temperatures in ambient mantle and plumes: constraints from basalts, picrites and komatiites. Geochem. Geophys. Geosyst. 8, 6–20.

Herzberg, C., O'Hara, M.J., 2002. Plume-associated ultramafic magmas of Phanerozoic age. J. Petrol. 43, 1857–1883.

Hickey-Vargas, R., Savov, I.P., Bizimis, M., Ishii, T., Fujioka, K. 2006. Origin of diverse geochemical signatures in igneous rocks from the Wet Philippine Basin: Implications for tectonic models D. Christie (Ed.), Back-Arc Spreading Systems: Geological, Biological, Chemical and Physical Interactions, AGU Geophysical Monograph, pp. 287–303.

Holland, T.J.B., Powell, R., 2011. An improved and extended internally-consistent thermodynamic dataset for phases of petrological interest, involving a new equation of state for solids. J. Metamorphic Geol. 29, 333–383.

Holland, T.J.B., Green, E.C.R., Powell, R., 2018. Melting of peridotites through to granites: A simple thermodynamic model in the system KNCFMASHTOCr. J. Petrology 59, 881–900.

Ikeda, Y., 1990. CeN/SrN/SmN; a trace element discriminant for basaltic rocks from different tectonomagmatic environments. N. Jb. Miner. Mh. Jg. 4, 145–159.

Ionov, D.A., Hofmann, A.W., 1995. Nb–Ta-rich mantle amphiboles and micas: implications for subduction-related metasomatic trace element fractionations. Earth Planet. Sci. Lett. 131, 341–356.

Irvine, T.N., Baragar, W.R.A., 1971. A Guide to the Chemical Classification of the Common Volcanic Rocks. Canad. J. Earth Sci. 8, 523–548.

Jenner, G.A., 1996. Trace element geochemistry of igneous rocks: Geochemical nomenclature and analytical geochemistry, in Trace Element Geochemistry of

Volcanic Rocks: Applications for Massive Sulfide Exploration, (Ed.) D.A. Wyman; Geological Association of Canada, Short Course Notes 12, 51–77.
Jennings, E.S., Holland, T.J.B., 2015. A simple thermodynamic model for melting of peridotite in the system NCFMASOCr. J. Petrol. 56, 869–892.
Johnson, P.R., Kattan, F.H., Al-Saleh, A.M., 2004. Neoproterozoic ophiolites in the Arabian Shield. In: Kusky TM (Ed.), Precambrian ophiolites and related rocks. In: Developments in Precambrian geology 13, Elsevier, 129–162.
Johnson, K.T.M., Sinton, J.M., 1990. Petrology, tectonic setting and the formation of back-arc basin basalts in the North Fiji Basin. Geol. Jahrb. 92, 517–545.
Johnson, P.R., Andresen, A., Collins, A.S., Fowler, A.R., Fritz, H., Ghebreab, W., Kusky, T., Stern, R.J., 2011. Late Cryogenian-Ediacaran history of the Arabian-Nubian Shield: a review of deposition, plutonic, structural, and tectonic events in the closing stages of the northern East African Orogen. J. Afr. Earth Sci. 61, 167–232.
Johnson, P.R., Woldehaimanot, B., 2003. Development of the Arabian-Nubian Shield: Perspectives on accretion and deformation in the East African Orogen and the assembly of Gondwana. In: Yoshida, M., Windley, B.F., Dasgupta, S. (Eds.), Proterozoic East Gondwana: supercontinent assembly and breakup. Publ Geol. Soc. Lond. Spec., pp. 289–325
Jung, C., Jung, S., Hoffer, E., Berndt, J., 2006. Petrogenesis of Tertiary mafic alkaline magmas in the Hocheifel, Germany. J. Petrol. 47, 1637–1671.
Katz, R., Spiegelman, M., Langmuir, C., 2003. A new parameterization of hydrous mantle melting. Geochem. Geophys. Geosyst. 4 https://doi.org/10.1029/2002GC000433.
Kelemen, P.B., Shimizu, N., Dunn, T., 1993. Relative depletion of niobium in some arc magmas: partitioning of K, Nb, La and Ce during melt–rock reaction in the upper mantle. Earth Planet. Sci. Lett. 120, 111–134.
Kelley, K.A., Cottrell, E., 2009. Water and the oxidation state of subduction zone magmas. Science 325, 605–607.
Khalil, A.E.S., Azer, M.K., 2007. Supra-subduction affinity in the Neoproterozoic serpentinites in the Eastern Desert, Egypt: Evidence from mineral composition. J. Afr. Earth Sci. 49, 136–152.
Kinzler, R.J., 1997. Melting of mantle peridotite at pressures approaching the spinel to garnet transition: application to mid-ocean ridge basalt petrogenesis. J. Geophys. Res. 102, 853–874.
Koutsovitis, P., Magganas, A., 2016. Boninitic and tholeiitic basaltic lavas and dikes from dispersed Jurassic East Othris ophiolitic units, Greece: petrogenesis and geodynamic implications. Int. Geol. Rev. 58, 1983–2006.
Kröner, A., Stern, R.J., 2004. Africa: Pan-African orogeny. In: Shelley, R., Cocks, L.R.M., Pilmer, I.R. (Eds.), Encyclopedia of Geology. Elsevier, Amsterdam, pp. 1–12.
Kröner, A., Todt, W., Hussein, I.M., Mansour, M., Rashwan, A.A., 1992. Dating of late Proterozoic ophiolites in Egypt and Sudan using the single grain zircon evaporation technique. Precam. Res. 59, 15–32.
Kusky, T.M., Abdelsalam, M., Tucker, R., Stern, R.J., 2003. Evolution of the East African and related Orogens, and the assembly of Gondwana. Precamb. Res. 123, 81–344.
Lambart, S., Laporte, D., Provost, A., Schiano, P., 2012. Fate of pyroxenite-derived melts in the peridotitic mantle: thermodynamic and experimental constraints. J. Petrol. 53, 451–476.
Langmuir, C.H., Bézos, A., Escrig, S., Parman, S.W., 2006. Chemical systematics and hydrous melting of the mantle in back-arc basins, in Back-Arc Spreading Systems: Geological, Biological, Chemical, and Physical Interactions. Geophys. Monogr. Ser. 166, 87–146.
Le Maitre, R.W., Bateman, P., Dudek, A., Keller, J., Lameyre, J., Le Bas, M.J., Sabine, P. A., Schmid, R., Sorensen, H., Streckeisen, A., Woolley, A.R., Zanettin, B., 1989. A Classification of Igneous Rocks and Glossary of Terms: Recommendations of the International Union of Geological Sciences Subcommission on the Systematics of Igneous Rocks. Blackwell Scientific, Oxford.
Lee, C.-T., Luffi, P., Plank, T., Dalton, H., Leeman, W.P., 2009. Constraints on the depths and temperatures of basaltic magma generation on Earth and other terrestrial planets, using new thermobarometers for mafic magmas. Earth Planet. Sci. Lett. 279, 20–33.
Leterrier, J., Mauru, R.C., Thonon, P., Girard, D., Marchal, M., 1982. Clinopyroxene composition as a method of identification of the magmatic affinities of paleo-volcanic series. Earth Planet. Sci. Lett. 9, 139–154.
Loucks, R.R., 1990. Discrimination of ophiolitic from nonophiolitic ultramafic–mafic allochthons in orogenic belts by the Al/Ti ratio in clinopyroxene. Geology 18, 346–349.
Makroum, F., 2017. Structural interpretation of the Wadi Hafafit culmination: A Pan-African gneissic dome in the central Eastern Desert, Egypt. Lithosphere 9, 759–773. https://doi.org/10.1130/L645.1.
Mather, K.A., Pearson, D.G., McKenzie, D., Kjarsgaard, B.A., Priestley, K., 2011. Constraints on the depth and thermal history of cratonic lithosphere from peridotite xenoliths, xenocrysts and seismology. Lithos 125, 729–742.
McKenzie, D.P., 1977. The initiation of trenches: A finite amplitude instability. In: Talwani M., Pitman, W.C., (Eds.), Island Arcs, Deep Sea Trenches and Back-Arc Basins. American Geophysical Union Maurice Ewing Series 1, pp. 57 – 61.
McKenzie, D.P., O'Nions, R.K., 1991. Partial melt distributions from inversion of rare-earth element concentrations. J. Petrol. 32, 1021–1091.
McKenzie, D.P., O'Nions, R.K., 1995. The source regions of ocean island basalts. J. Petrol. 36, 133–159.
Metzger, E.P., Miller, R.B., Harper, G.D., 2002. Geochemistry and tectonic setting of the ophiolitic Ingalls complex, North Cascades, Washington: implications for Correlations of Jurassic Cordilleran Ophiolites. J. Geol 110, 543–560.
Morimoto, N., 1988. The Nomenclature of Pyroxenes. Mineral. Mag. 52, 425–433.
Nielsen, R.L., Dungan, M.A., 1983. Low pressure mineral-melt equilibria in natural anhydrous mafic systems. Contrib. Mineral. Petrol. 84, 310–326.
Nimis, P.A., 1995. Clinopyroxene geobarometer for basaltic systems based on crystal-structure modeling. Contrib. Mineral. Petrol. 121, 115–125.
Nimis, P., Ulmer, P., 1998. Clinopyroxene Geobarometry of Magmatic Rocks Part 1: An Expanded Structural Geobarometer for Anhydrous and Hydrous, Basic and Ultrabasic Systems. Contrib. Mineral. Petrol. 133, 122–135.
Nimis, P., Taylor, W.R., 2000. Single-clinopyroxene thermobarometry for garnet peridotites. Part I. Calibration and testing of a Cr-in-Cpx barometer and an enstatite-in-Cpx thermometer. Contrib. Mineral. Petrol. 139, 541–554.
Murphy, J.B., Hynes, A.J., 1986. Contrasting mobility of Ti, P, Zr, Nb, and Y in two suites of metabasaltic rocks in the Canadian Appalachians. Can. J. Earth Sci. 23, 1147–1153.
Parlak, O., Höck, V., Delaloye, M., 2002. The Suprasubduction Pozanti-Karsanti Ophiolite, Southern Turkey: Evidence for High Pressure Crystal Fractionation of Ultramafic Cumulates. Lithos 65, 205–224.
Pearce, J.A., Norry, M.J., 1979. Petrogenetic implications of Ti, Zr, Y, and Nb variations in volcanic rocks. Contrib. Mineral. Petrol. 69, 33–47.
Pearce, J.A., Wyman, D.A.A., 1996. Users guide to basalt discrimination diagrams, Trace Element Geochemistry of Volcanic Rocks: Applications for Massive Sulphide Exploration. Geol. Assoc. Canada, Short Course Notes 12, 79–113.
Pearce, J.A., Robinson, R.B., 2011. Strategic Management: Formulation, Implementation and Control. McGraw Hill, New York.
Pearce, J.A., 2008. Geochemical fingerprinting of oceanic basalts with applications to ophiolite classification and the search for the Archean oceanic crust. Lithos 100, 14–48.
Pearce, J.A., Peate, D.W., 1995. Tectonic implications of the composition of volcanic ARC magmas. Ann. Rev. Earth Planet. Sci. 23, 251–285.
Plank, T., 2005. Constraints from Th/La on sediment recycling at subduction zones and the evolution of the continents. J. Petrol. 46, 921–944.
Plank, T., Kelley, K.A., Zimmer, M.M., Hauri, E.H., Wallace, P.J., 2013. Why do mafic arc magmas contain~ 4 wt% water on average? Earth Planet Sci. Lett. 364, 168–179.
Plank, T., Langmuir, C.H., 1992. Effects of the melting regime on the composition of the oceanic crust. J. Geophys. Res. 97, 19749–19770.
Plank, T., Langmuir, C.H., 1998. The geochemical composition of subducting sediment and its consequences for the crust and mantle. Chem. Geol. 145, 325–394.
Price, R.C., Johnson, L.E., Crawford, A.J., 1990. Basalts of the North Fiji Basin: the generation of back arc basin magmas by mixing of depleted and enriched mantle sources. Contrib. Mineral. Petrol. 105, 106–121.
Putirka, K., 2008. Thermometers and Barometers for Volcanic Systems. Rev. in Mineral. Geochem. 69, 61–120.
Putirka, K.D., Mikaelian, H., Ryerson, F., Shaw, H., 2003. New clinopyroxene-liquid thermobarometers for mafic, evolved, and volatile-bearing lava compositions, with application to lavas from Tibet and the Snake River Plain, Idaho. Am. Mineral. 88, 1542–1554.
Putirka, K.D., Perfit, M., Ryerson, F.J., Jackson, M.G., 2007. Ambient and excess mantle temperatures, olivine thermometry, and active vs. passive upwelling. Chem. Geol. 241, 177–206.
Reagan, M.K., Meijer, A., 1984. Geology and geochemistry of early arc-volcanic rocks from Guam. Geol. Soc. Am. Bull. 95, 701–713.
Robinson, P.T., Malpas, J., Dilek, Y., Zhou, M., 2008. The significance of sheeted dike complexes in ophiolites. GSA Today 18 (11). https://doi.org/10.1130/GSATG22A.1.
Rogkala, A., Petrounias, P., Tsikouras, B., Giannakopoulou, P.P., Hatzipanagiotou, K., 2019. Mineralogical Evidence for Partial Melting and Melt-Rock Interaction Processes in the Mantle Peridotites of Edessa Ophiolite (North Greece). Minerals 9, 120.
Rolland, Y., Pecher, A., Picard, C., 2000. Mid-Cretaceous Back-ˆarc formation and Arc evolution along the Asian margin: the Shyok Suture Zone in northern Ladakh NW Himalaya. Tectonophysics 325, 145–173.
Ross, P.S., Bédard, J.H., 2009. Magmatic affinity of modern and ancient subalkaline volcanic rocks determined from trace-element discriminant diagrams Canad. Earth Sci. 46, 823–839.
Rudnick, R.L., Gao, S., 2003. The Composition of the Continental Crust. In: Holland, H. D., Turekian, K.K. (Eds.), Treatise on Geochemistry 3, 1-64.
Saccani, E., 2015. A new method of discriminating different types of post Archean ophiolitic basalts and their tectonic significance using Th-Nb and Ce-Dy-Yb systematics. Geosci. Front. 6, 481–501.
Saccani, E., Delavari, M., Dolati, A., Marroni, M., Pandolfi, L., Chiari, M., Barbero, E., 2018. New insights into the geodynamics of Neo-Tethys in the Makran area: evidence from age and petrology of ophiolites from the Coloured Mélange Complex (SE Iran). Gondwana Res. 62, 306–327.
Saunders, A.D., Norry, M.J., Tarney, J., 1988. Origin of MORB and chemically depleted mantle reservoirs: Trace element constrains. In: Menzies, M.A., Cox, K.G. (Eds.), Oceanic and continental lithosphere: Similarities and Differences, J. Petrol., V. Special Volume, 415–445.
Shackleton, R.M., 1994. Review of late Proterozoic sutures, ophiolitic mélanges and tectonics of eastern Egypt and north Sudan. Geol. Rundsch. 83, 537–546.
Shaw, D.M., 2000. Continuous (dynamic) melting theory revisited. Can. Mineral. 38, 1041–1063.
Sinton, J.M., Ford, L.L., Chappell, B., McCulloch, M.T., 2003. Magma genesis and mantle heterogeneity in the Manus back-arc basin, Papua New Guinea. J. Petrol. 44, 159–195.
Smith, G.P., Wiens, D.A., Fischer, K.M., Dorman, L.M., Webb, S.C., Hildebrand, J.A., 2001. A complex pattern of mantle flow in the Lau backarc. Science 292, 713–716.
Soto, J.I., Soto, V.M., 1995. Ptmafic: Software package for thermometry, barometry, and activity calculations in mafic rocks using an IBM-compatible computer. Comput. Geosci. 21, 619–652.
Stern, C., de Wit, M.J., 2003. Rocas Verdes ophiolites, southernmost South America: Remnants of progressive stages of development of oceanic-type crust in a continental

margin back-arc basin. In: Dilek, Y., Robinson, P.T. (Eds.), Ophiolites in Earth History. Geol Soc. London Spec. Publ. 218, 665–683.
Stern, R.J., Johnson, P., Kroner, A., Yibas, B., 2004. Neoproterozoic ophiolites of the Arabian-Nubian Shield. In Kusky, T. M., ed. Precambrian ophiolites and related rocks. Devel. Precam. Geol. 13, 95–128.
Sun, S.S., Mcdonough, W.F., 1989. Chemical and isotopic systematics of oceanic basalts: implications for mantle composition and processes. In: Saunders, A.D., Norry, M.J. (Eds.), Magmatism in the Ocean Basins. Geol. Soc. London, Spec. Publ. 42, 313–345.
Sun, S.S., Nesbitt, R.W., 1977. Chemical heterogeneity of the Archaean mantle, composition of the earth and mantle evolution. Earth Planet. Sci. Lett. 35, 429–448.
Sun, S.S., Nesbitt, R.W., 1978. Geochemical regularities and genetic significance of ophiolitic basalts. Geology 28, 689–693.
Tatsumi, Y., Ishizaka, K., 1982. Origin of high magnesian andesites in the Setouchi Volcanic belt, southwest Japan, I. Petrographical and chemical characteristics. Earth Planet. Sci. Lett. 60, 293–304.
Thirlwall, M.F., Anczkiewicza, R., 2004. Multidynamic isotope ratio analysis using MC-ICP-MS and the causes of secular drift in Hf, Nd and Pb isotope ratios. Int. J. Mass Spectrom. 235, 59–81.
Toth, J., Gurnis, M., 1998. Dynamics of subduction initiation at pre-existing fault zones. J. Geophy. Res. 103, 18053–18067.
Tsikouras, B., Karipi, S., Rigopoulos, I., Perraki, M., Pomonis, P., Hatzipanagiotou, K., 2009. Geochemical processes and petrogenetic evolution of rodingite dikes in the ophiolite complex of Othrys (Central Greece). Lithos 113, 540–554.
van Hinsbergen, D.J.J., Peters, K., Maffione, M., Spakman, W., Guilmette, C., Thieulot, C., Plümper, O., Gürer, D., Brouwer, F.M., Aldanmaz, E., Kaymakcı, N., 2015. Dynamics of intraoceanic subduction initiation: 2. Suprasubduction zone ophiolite formation and metamorphic sole exhumation in context of absolute plate motions. Geochem. Geophys. Geosys. 16, 1771–1785.
Whattam, S.A., Stern, R.J., 2011. The 'subduction initiation rule': a key for linking ophiolites, intra-oceanic forearcs and subduction initiation. Contrib. Mineral. Petrol. 162, 1031–1045.
Whitney, D.L., Evans, B.W., 2010. Abbreviations for names of rock-forming minerals. Am. Mineral. 95, 185–187.
Wood, D.A., 1980. The application of a Th–Hf–Ta diagram to problems of tectonomagma classification and establishing the nature of crustal contamination of basaltic lavas of the British Tertiary volcanic province. Earth Planet. Sci. Lett. 50, 11–30.
Workman, R.K., Hart, S.R., 2005. Major and trace element composition of the depleted MORB mantle (DMM). Earth Planet Sci. Lett. 231, 53–72.
Yavuz, F., 2013. WinPyrox: A Windows program for pyroxene calculation classification and thermobarometry. Am. Mineral. 98, 1338–1359.
Ziberna, L., Nimis, P., Kuzmin, D., Malkovets, V.G., 2016. Error sources in single-clinopyroxene thermobarometry and a mantle geotherm for the Novinka kimberlite, Yakutia. Am. Mineral. 101, 2222–2232.
Zimmer, M., Kroner, A., Jochum, K.P., Reishmann, T., Todt, W., 1995. The Gabal Gerf complex: a Precambrian N-MORB ophiolite in the Nubian Shield, NE Africa. Chem. Geol. 128, 29–51.
Zimmer, M.M., Plank, T., Hauri, E.H., Yogodzinski, G.M., Stelling, P., Larsen, J., Singer, B., Jicha, B., Mandeville, C., Nye, C.J., 2010. The Role of Water in Generating the Calc-alkaline Trend: New Volatile Data for Aleutian Magmas and a New Tholeiitic Index. J. Petrol. 51 (12), 2411–2444. https://doi.org/10.1093/petrology/egq062.
Zoheir, B.A., Klemm, D.D., 2007. The tectonometamorphic evolution of the central part of the Neoproterozoic Allaqi-Heiani suture, south Eastern Desert of Egypt. Gondwana Res. 12, 287–304.